AD-A182 867 THE EFFECT OF PROCESSING AND SUPERPLASTIC DEFORMATION ON AMBIENT DUCTILITY OF AL-10XMG-01XZR(U) NAVAL POSTGRADUATE SCHOOL MONTEREY CA D K SOLOMOS MAR 87 1/1

UNCLASSIFIED F/G 11/6.1 NL

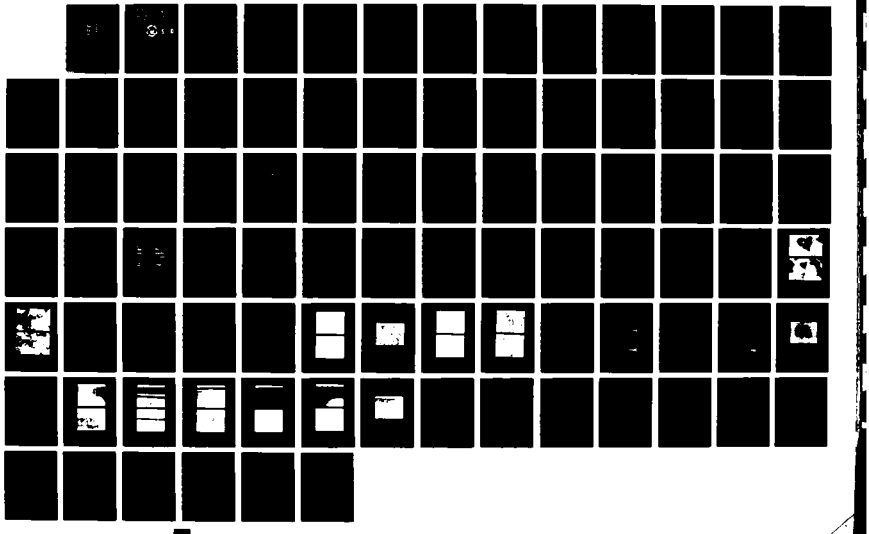

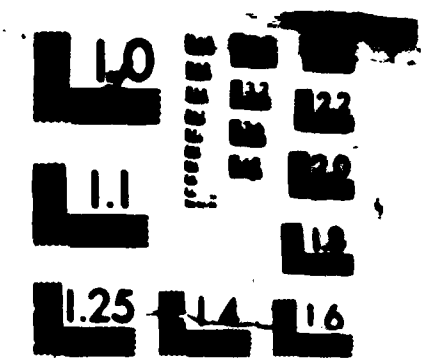

MICROCOPY RESOLUTION TEST CHART

NAVAL POSTGRADUATE SCHOOL
Monterey, California

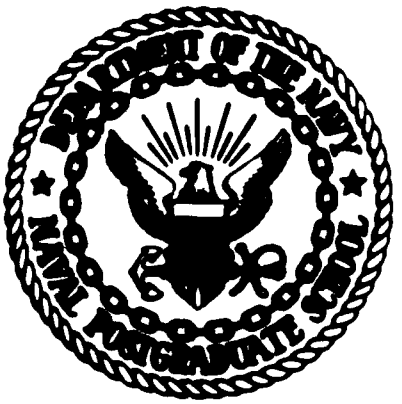

THESIS

THE EFFECT OF
PROCESSING AND SUPERPLASTIC DEFORMATION
ON AMBIENT DUCTILITY OF Al-10%Mg-0.1%Zr

by

Dimosthenis K. Solomos

March 1987

Thesis Advisor: T.R. McNelley

A182 067

SECURITY CLASSIFICATION OF THIS PAGE

REPORT DOCUMENTATION PAGE

1a REPORT SECURITY CLASSIFICATION UNCLASSIFIED	1b RESTRICTIVE MARKINGS
2a SECURITY CLASSIFICATION AUTHORITY	3 DISTRIBUTION/AVAILABILITY OF REPORT Approved for public release; distribution is unlimited.
2b DECLASSIFICATION/DOWNGRADING SCHEDULE	
4 PERFORMING ORGANIZATION REPORT NUMBER(S)	5 MONITORING ORGANIZATION REPORT NUMBER(S)
6a NAME OF PERFORMING ORGANIZATION Naval Postgraduate School 6b OFFICE SYMBOL (If applicable) 69	7a NAME OF MONITORING ORGANIZATION Naval Postgraduate School
6c ADDRESS (City, State, and ZIP Code) Monterey, California 93943-5000	7b ADDRESS (City, State, and ZIP Code) Monterey, California 93943-5000
8a NAME OF FUNDING/SPONSORING ORGANIZATION 8b OFFICE SYMBOL (If applicable)	9 PROCUREMENT INSTRUMENT IDENTIFICATION NUMBER
8c ADDRESS (City, State, and ZIP Code)	10 SOURCE OF FUNDING NUMBERS PROGRAM ELEMENT NO / PROJECT NO / TASK NO / WORK UNIT ACCESSION NO

11 TITLE (Include Security Classification)
THE EFFECT OF PROCESSING AND SUPERPLASTIC DEFORMATION ON AMBIENT DUCTILITY OF Al-10%Mg-0.1%Zr

12 PERSONAL AUTHOR(S)
Solomos, Dimosthenis K.

13a TYPE OF REPORT	13b TIME COVERED FROM ____ TO ____	14 DATE OF REPORT (Year Month Day)	15 PAGE COUNT
Master's Thesis		1987 March	87

16 SUPPLEMENTARY NOTATION

17 COSATI CODES		
FIELD	GROUP	SUB-GROUP

18 SUBJECT TERMS (Continue on reverse if necessary and identify by block number)
Superplasticity, Ductility, Aluminum-Magnesium Alloys, Thermomechanical Processing, Aluminum Alloys

19 ABSTRACT (Continue on reverse if necessary and identify by block number)

In previous work, the room temperature mechanical properties of an Al-10Mg-0.1Zr alloy were evaluated after simulated, superplastic forming at a temperature of 300°C (573K). A variation of ductility from 1 to 14% elongation was observed in the room temperature test data. To examine the cause of this variability, the processing schedule was changed to one incorporating more severe reductions during rolling. This resulted in a lesser range of variability in room temperature ductility, but the material no longer behaved superplastically. Elongations at 300°C of only 161% at a maximum were recorded although the small grain size

20 DISTRIBUTION/AVAILABILITY OF ABSTRACT	21 ABSTRACT SECURITY CLASSIFICATION
☒ UNCLASSIFIED/UNLIMITED ☐ SAME AS RPT ☐ DTIC USERS	UNCLASSIFIED
22a NAME OF RESPONSIBLE INDIVIDUAL Terry McNelley	22b TELEPHONE (Include Area Code) (408) 646-2589 22c OFFICE SYMBOL 69Mc

DD FORM 1473, 84 MAR 83 APR edition may be used until exhausted
All other editions are obsolete

SECURITY CLASSIFICATION OF THIS PAGE

contd

(19. continued)
required for good superplasticity apparently was developed. SEM and optical microscopy was then done to investigate the cause of this loss of superplastic behavior.

(Keywords:)

Approved for public release; distribution is unlimited.

The Effect of Processing and Superplastic Deformation on Ambient Ductility of Al-10%Mg-0.1%Zr

by

Dimosthenis K. Solomos
Commander, Hellenic Navy
B.S., Greek Naval Academy, 1968

Submitted in partial fulfillment of the requirements for the degree of

MASTER OF SCIENCE IN MECHANICAL ENGINEERING

from the

NAVAL POSTGRADUATE SCHOOL
March 1987

Author: _____
Dimosthenis K. Solomos

Approved by: _____
T.R. McNelley, Thesis Advisor

_____
A.J. Healey, Chairman, Department of Mechanical Engineering

_____
Gordon E. Schacher, Dean of Science and Engineering

ABSTRACT

In previous work, the room temperature mechanical properties of an Al-10Mg-0.1Zr alloy were evaluated after simulated, superplastic forming at a temperature of 300°C (573K). A variation of ductility from 1 to 14% elongation was observed in the room temperature test data. To examine the cause of this variability, the processing schedule was changed to one incorporating more severe reductions during rolling. This resulted in a lesser range of variability in room temperature ductility, but the material no longer behaved superplastically. Elongations at 300°C of only 161% at a maximum were recorded although the small grain size required for good superplasticity apparently was developed. SEM and optical microscopy was employed to investigate the cause of this loss of superplastic behavior.

TABLE OF CONTENTS

LIST OF TABLES

LIST OF FIGURES

ACKNOWLEDGEMENT

I would like to thank my advisor, Professor T.R. McNelley, and Dr. S.J. Hales for their expert assistance and guidance in conducting this research. Also I thank T. McCord, T. Kellogg and Tamara Bloomer, whose technical expertise, material support and knowledge were vital to me in the experimental portion of this thesis. I would also like to acknowledge the Hellenic Navy for the opportunity given me to attend the Naval Postgraduate School and obtain the Master degree. Finally, I would like to express my sincere appreciation to my wife Marika and our two children Olga and Constantinos for their dedicated support of my work at NPS.

I. INTRODUCTION

The phenomenon of superplasticity, as Sherby and Wadsworth [Ref. 1] have pointed out, was first reported by Bengough [Ref. 2] as "enormous elongations" attained as early as 1912 in a specially processed brass. In 1920, Rosenhain [Ref. 3] demonstrated for the first time the phenomenon of superplasticity in a cold-rolled zinc:copper: aluminum ternary eutectic alloy. However, the discovery of superplasticity is most often attributed to Pearson [Ref. 4] in 1934. Since then, a large amount of research has been accomplished, and much remains to be learned about the mechanisms that facilitate deforming of a material in tension at very low stresses with essentially, neck-free elongations of several hundred to perhaps several thousand percent. For example, 5550% elongation has been reported by Higashi and co-workers [Ref. 5]. According to Sherby and Wadsworth [Ref.1], ductility in tension above 200% elongation to fracture is considered superplastic and many superplastic alloys exhibit optimum elongations of 500 to 1000%.

In recent years, there has been an increased interest in superplastic aluminum alloys not only for commercial but also for military use. This interest has arisen because of the many opportunities for application that these materials

possess, such as: (1) application of plastics industry forming methods to metals; (2) ability to fabricate complex shapes from a single piece of metal; (3) elimination of fasteners and welds in high strength components with complicated geometry and therefore weight savings as well as improved fatigue and corrosion resistance, as such degradation often begins at fastener holes or joints; (4) production of structural components requiring a combination of high strength, light weight and good ductility.

Research at the Naval Postgraduate School (NPS) has concentrated on high-Magnesium Aluminum-Magnesium alloys with the primary goal to determine mechanisms responsible for superplasticity as well as which of these high-strength, light-weight Al-Mg alloys might be suitable for airframe constructions. The choice of high-Magnesium content evolved from previous research at the NPS [Ref.6-17]. Recent research [Ref. 18-22] has focused on the Al-10%Mg-0.1%Ar alloy to investigate the mechanical properties of this superplastic alloy. Klankowski [Ref. 21] and Grider [Ref. 22] evaluated the room temperature mechanical properties of this Al-10%Mg-0.1%Zr alloy, after simulated, warm temperature (300°C) superplastic forming. A variation of ductility from 1 to 14% elongation was observed in the room temperature data.

The present research was intended to examine the cause of this variability. The processing schedule was changed to

one incorporating more severe reduction during rolling. This resulted in a lesser range of room temperature variability but the material no longer behaved superplastically at warm temperatures although the fine grain size required for good superplasticity apparently was developed.

This thesis presents the data obtained from the tensile tests and the microstructural examination conducted using TEM, SEM and optical microscopy. Review of this work and new questions are posed for subsequent investigation.

II. BACKGROUND

A. ALUMINUM-MAGNESIUM ALLOYS

Aluminum alloys have been extensively studied because of their low density, good ductility, potential for a high strength-to-weight ratio, good fracture toughness and corrosion resistance. Most of the higher-strength aluminum alloys obtain their strength through precipitation and solid solution hardening. Precipitation strengthening refers to the retardation of dislocation motion by dispersed particles. Solid solution strengthening is due to the retardation of the dislocation motion because of the solute interaction with the stress fields of dislocations. In addition, dislocation substructures resulting from deformation present barriers to subsequent dislocation motion and this constitutes strain hardening.

The aluminum-magnesium alloy system has been studied extensively at the Naval Postgraduate School (NPS). Figure 2.1 shows the aluminum-magnesium binary phase diagram. For alloys containing up to 6% Mg and processed under ordinary conditions, most of the Mg present may be retained in solution and therefore strengthening is primarily by the solid solution mechanism with possibly strain hardening as well. Beyond 6% Mg, the β (Mg_5Al_8), will have an increased tendency to form; while precipitation hardening may result

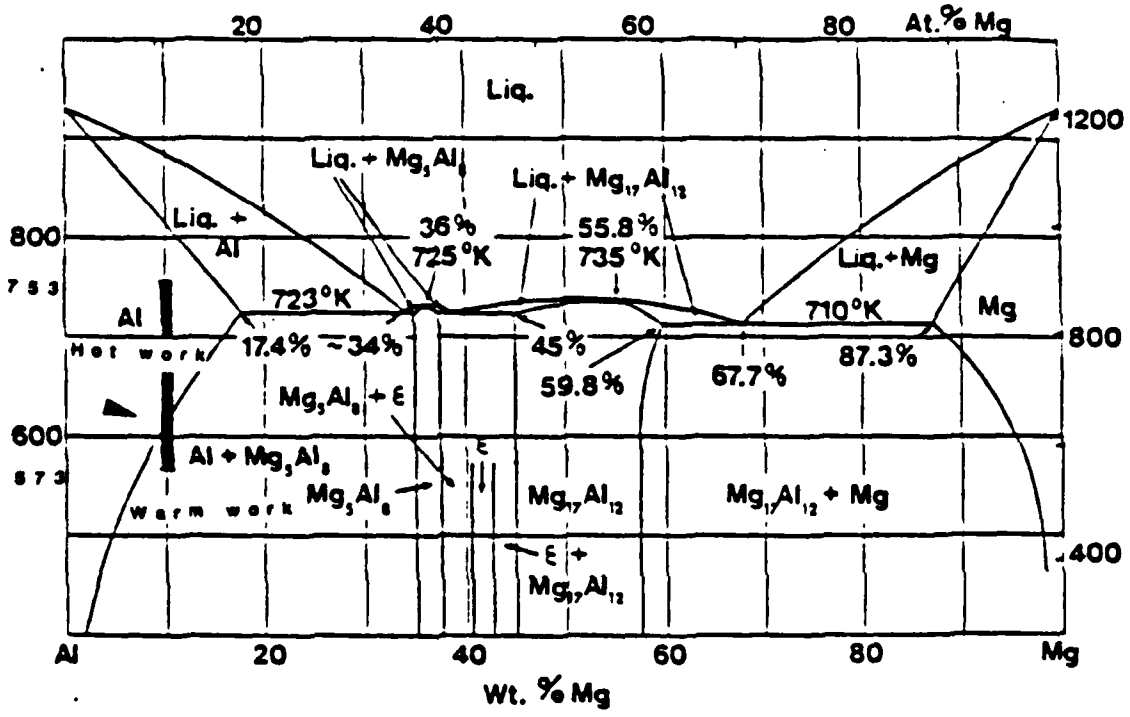

Figure 2.1. Phase Diagram for the Aluminum-Magnesium System

from the formation of β, uncontrolled precipitation of the β on grain boundaries may leave the alloy in a condition susceptible to stress-corrosion cracking. Thus, warm-working of the alloy used in this study containing 10 wt% Mg at a temperature below Mg-solvus but above 200°C induces precipitation of the β phase and results in a more homogeneous distribution of the β. Also, the processing increases the strength through a combination of the precipitation, strain and solid solution hardening mechanisms.

It is widely accepted that superplastic behavior requires an equiaxed structure of a uniformly fine grain size, typically less than 10 microns. Such a microstructure is most commonly produced by mechanical working of the material and then recrystallizing at elevated temperature. Often, however, rapid microstructural coarsening also occurs at such temperatures. Clearly then, some form of grain refinement is necessary if the elevated temperature fine grain size requirements for superplastic deformation are to be met.

A refined and stabilized structure may be obtained by the addition of dispersoid-forming elements such as Mn or Zr, as in this work. The most important effect of Zr addition is that it controls the extent to which recrystallization can occur during elevated temperature processing [Ref. 27]. Inhibiting the recrystallization has

the effect of slowing the rate of microstructural coarsening and this is beneficial in controlling the superplastic properties of the aluminum alloy.

B. SUPERPLASTIC BEHAVIOR

1. Phenomenological Considerations

Superplastic behavior is found in materials in which the strength is highly strain rate sensitive. In analysis of deformation at high temperature, flow stress is related to the strain rate by a power law relation:

$$\sigma = K\dot{\epsilon}^m \qquad \text{(eqn. 2.1)}$$

where σ is the flow stress, K is a microstructure and temperature-dependent material constant, $\dot{\epsilon}$ is the strain rate and m is the strain rate sensitivity coefficient. The coefficient m may also be defined as:

$$m = \frac{d(\ln \sigma)}{d(\ln \dot{\epsilon})} \qquad \text{(eqn. 2.2)}$$

It is usually experimentally determined from a log-log plot of stress versus strain rate for the material of concern. The range of m-value for superplastic materials usually is from 0.3 to 0.7. As m increases, resistance to necking increases and consequently greater ductility results. When the relation between σ and ϵ is linear (m=1), the material is said to behave in a Newtonian-viscous manner; hot glass, tar, and well-masticated chewing gum all obey the

Newtonian-viscous relationship, and these materials can be classified as ideally superplastic [Ref. 1].

Various theoretical models have been proposed to explain superplasticity. These fall generally into two categories: those relying on diffusional processes alone and those modeled on dislocation deformation processes. Models based on established creep mechanisms are often proposed, where superplastic deformation is to be thought of as an exaggerated form of creep.

Explanations for superplastic response commonly divide the stress versus strain-rate curve into three regions, each being dominated by a different mechanism (Figure 2.2). The existence of Region I, which is not always observed experimentally, is disputed [Ref. 36]. Region II, with the largest m value, is where the greatest elongations occur. A typical m value reported in the literature is 0.5. The deformation mechanism in this region is generally accepted to be some form of grain boundary sliding. The most prevalent model to explain the grain boundary sliding was proposed by Ashby and Verrall, Figure 2.3 [Ref. 28]. More recently, Ruano and Sherby [Ref. 29] have shown that results more consistent with reported data are obtained by modeling superplastic deformation as grain boundary sliding accommodated by slip. At high stresses in Region III, it is generally accepted that the dislocation mechanisms dominate.

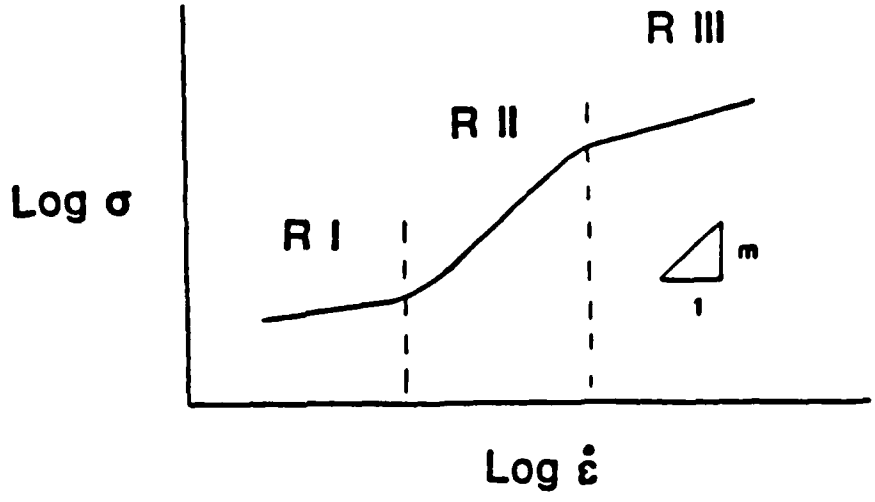

Figure 2.2. Typical plot of log σ vs log $\dot{\varepsilon}$ obtained from constant strain rate data. In $\sigma = B\,\dot{\varepsilon}^m$, m, the slope, is the strain rate sensitivity coefficient.

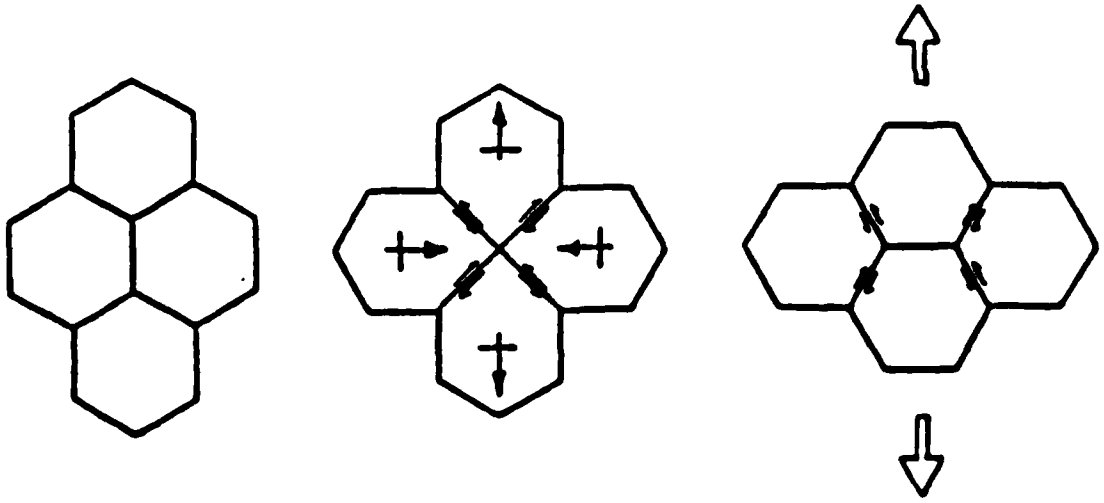

Figure 2.3. Illustration of the Ashby-Verrall model for grain boundary sliding with diffusional accommodation [Ref. 29].

The basic theory for creep that relies upon dislocation climb to overcome obstacles which otherwise prevent further elongation was formulated by Weertman [Ref. 30]. Both deformation mechanisms may operate simultaneously during deformation, but in Region II grain boundary sliding dominates, while in Region III the dislocation mechanism dominates. Equation 2.3 gives the total strain rate $\dot{\varepsilon}_{total}$ of deformation as the sum of a superplastic mechanism and a dislocation deformation mechanism:

$$\dot{\varepsilon}_{total} = K_1 \frac{D_{eff}\, b}{dP} \left[\frac{\sigma}{E}\right]^{1/m} + K_2 D_S \sigma^3 \qquad \text{(eqn 2.3)}$$

where k_1 and k_2 are constants, D_{eff} is the effective diffusion coefficient b is the burgers vector, σ is the applied stress, d is the grain size, p is the grain size exponent, E is the elastic modulus, m is the strain-rate sensitivity coefficient, and D_s is the diffusion coefficient for solute diffusion. The first term of the equation was proposed by Ruano and Sherby [Ref. 29] to describe the Region II, while the second term proposed by Weertman [Ref. 31] to describe Region III. Examination of Equation 2.3 reveals that the first term on the right-hand side dominates at lower stresses and strain rates; with increasing strain rate the second dominates, thus predicting the experimentally observed transition from a superplastic mechanism (Equation 2.3 is thought to describe grain boundary sliding) to a dislocation deformation process.

2. Microstructural Considerations

Superplasticity is the ability of a material to deform to at least 200% tensile elongation without fracture. It is generally agreed that there are certain prerequisites for superplasticity. These include: 1) high angle grain boundaries, since the predominant mode of deformation during superplastic flow is grain boundary sliding; the grain boundaries must be mobile to relieve stress concentrations resulting from the grain boundary sliding, and equiaxed to better accommodate the grain rotation that accompanies the grain boundary sliding; 2) a fine grain size which will enhance the contribution of the superplastic response; 3) a second phase, which is generally necessary to retard grain growth and must deform with the matrix and be uniformly distributed.

3. Microstructural Transformations

There are a number of mechanisms which contribute to the transformation of a heavily deformed structure into a structure consisting of fine equiaxed grains. It is, therefore, necessary to define the terms relevant to this microstructural transformation before discussing processing methods used for achieving grain refinement.

a. Recovery

Recovery refers to the process where dislocation networks introduced during mechanical working rearrange themselves into lower energy configurations without

recrystallization or change in orientation of the crystal lattice. Such rearrangement is called polygonization when recovery results in a rearrangement of the dislocations into cellular arrays [Ref. 32]. The driving force for recovery is reduction of the large amount of stored energy introduced during working.

b. Recrystallization

Recrystallization is observed to occur by two distinct modes. Discontinuous is the classical recrystallization path that proceeds by nucleation of new grains in the deformation structure and growth of these grains by boundary migration until impingement. The large grain size that results raises flow stress rapidly and halts superplastic deformation; this can be seen in Equation 2.3, where a large grain size d will suppress the first term on the right-hand side. Such a microstructure may be unsuitable for superplastic deformation. Continuous recrystallization is an alternate recrystallization path which does not proceed by nucleation and growth of new grains with grain boundary migration. Instead, this mode occurs by a gradual process of subgrain coalescence, leading to formation of high-angle grain boundaries without high angle boundary migration [Ref. 23]. These high-angle boundaries are generally quite stable and resistant to coarsening. Hence, if a fine initial grain size can be established, it may be expected to exhibit good

microstructural stability, coarsening little with time. Therefore, continuous recrystallization seems capable of reconciling the requirements of fine grain size and elevated temperature stability necessary for superplastic deformation.

4. Processing Methods for Grain Refinement

Methods of achieving fine-grain size have centered around controlled thermomechanical processing. The microstructural prerequisites for superplasticity have been realized using subsequent heat treatments to transform a highly deformed microstructures into a fine-grained microstructure via a discontinuous recrystallization process. It was suggest by Wert [Ref. 23] that dynamic recrystallization will occur during hot working; this would assist in microstructural refinement and in achieving a more uniform distribution of the precipitate.

An alternative approach to attain grain refinement is that reported by McNelley, Lee and co-workers [Ref. 24-26]. This consists of processing an aluminum-magnesium alloy by warm rolling such that precipitation of intermetallic β (Al_8Mg_5) occurs concurrently with the formation of a highly refined structure. No recrystallization heat treatments were used prior to elevated temperature deformation and the materials exhibited a superplastic response while in an apparently non-recrystallized condition.

C. WHY THE PRESENT WORK

The principle focus of this work was on the ambient temperature ductility of the Al-10%Mg-0.1Zr alloy. Klankowski [Ref. 21] used a light rolling reduction processing scheme which resulted in good warm temperature superplasticity but ambient temperature ductilities which varied widely. Grider [Ref. 22] changed to a heavy rolling reduction scheme with a true strain ≈2 in warm rolling and concluded that the heavier reduction during rolling eliminated edge defects and improved the as-rolled ambient temperature ductility from 8 to 19%. This present work then sought to apply the greater total strain to investigate the results of Grider's [Ref. 22] work to study the effect of processing and superplastic deformation on ambient ductility of the alloy, as well as to determine the cause of the variability in room temperature ductility reported by Klankowski [Ref. 21].

III. EXPERIMENTAL PROCEDURE

A. MATERIAL

The aluminum alloy investigated was nominally 10%Mg and 0.1%Zr (wt.%). The direct-chill cast ingot was produced by ALCOA Technical Center using 99.99% pure aluminum bare metal alloyed with commercially pure magnesium, Aluminum-Zirconium master alloy, Ti-B addition for grain size control in the as-cast condition, and Beryllium as 5% Be Aluminum-Beryllium master alloy for oxidation control [Ref.33]. The as-received ingot measured 127 mm (5 in) in diameter and 1016 mm (44 in) in length. Table I lists the complete chemical composition of the alloy examined. [Ref. 33]

TABLE I

ALLOY COMPOSITION (wt%)

Serial Number	Si	Fe	Mg	Zr	Ti	Be	Al
572826	0.02	0.02	9.89	0.09	0.01	0.003	Balance

B. PROCESSING

Processing followed the sequence shown in Figure 3.1. The ingot was sectioned into billets 32 mm X 32 mm X 95 mm with a square cross section of width and thickness 32 mm (1.26 in). The procedure followed was that developed originally by Johnson [Ref.12] and refined by Becker [Ref. 14], where the billets were solution treated at

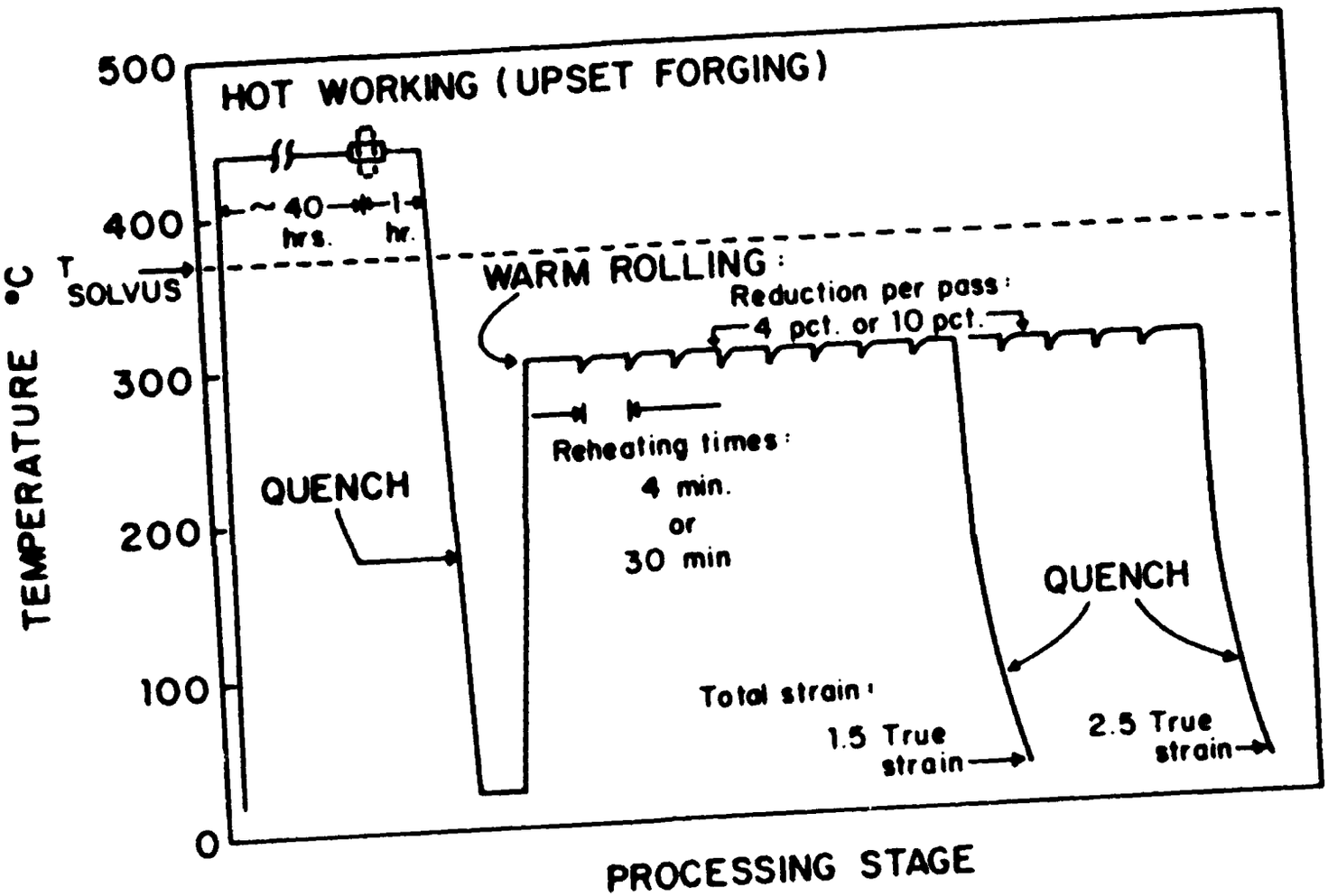

Figure 3.1. Thermomechanical Processing Technique.

440°C for 40 hours. The billets' surface temperatures were monitored with two thermocouples. Then they were upset forged on platens, heated to the solution treating temperature, to approximately 25.4 mm (1 in) in height. Subsequently, they were reheated to 440°C for one hour to assure uniform temperature above the Mg solvus and then oil quenched. The billets were forged longitudinally, resulting in a reduction of approximately 73%, equivalent to a true strain of about 1.3.

C. WARM ROLLING

The billets were then warm rolled into sheets within 24 hours of upset forging, following a reheating time and thickness reduction schedule which now will be referred to as the heavy reduction schedule (see also Wise [Ref. 35]). Each billet was divided equally in two parts. Each part was heated to 300°C for 30 minutes to achieve isothermal conditions prior to the first rolling pass. This was done to prevent cracking of forged billets due to uneven heating during the rolling process. To obtain the isothermal conditions each part was placed on a large steel plate, which acted as a heat sink in a preheated furnace. Using thermocouples the billet surface and steel plate temperature were monitored. The billet portion was then rolled following the heavy reduction scheme to a thickness of about 0.09 in. This required about 9 passes, resulting in a final warm reduction of approximately 92%, equivalent to a true

strain of about 2.5. Between each successive pass the sheet was returned to the furnace for four minutes to maintain isothermal conditions. Also, to reduce bowing the rolled sheet was rotated endwise after each pass, always maintaining the initial longitudinal direction. Figure 3.2 shows on a portion of the Al-Mg phase diagram where the hot and warm working were done.

D. SPECIMEN FABRICATION

For the simulated superplastic warm forming, two blanks were cut from each rolled sheet. The blank dimensions were 146 mm (5.75 in) in length by 33 mm (1.3 in) in width. These were machined to give nominal gage dimensions of 20.30 mm (0.800 in) width and 50.80 mm (2.00 in) length. This gave a gage width-to-length ratio of 1 to 2.5. Shoulder curvature for these specimens was 6.35 mm (0.25 in). Figure 3.3 shows this specimen geometry. Elongations were based on a 50.8 mm (2.0 in) gage length scribed on the specimens before warm deformation.

Following simulated superplastic forming, ambient temperature test blanks were cut from the gage sections of the warm-deformed specimens. Due to the small gage section width after the deformation, a reduced size ambient temperature test specimen blank, 66 mm (2.6 in) in length and 10 mm (0.4 in) in width to provide a test specimen of gage dimensions 5.08 mm (0.200 in) width by 20.30 mm

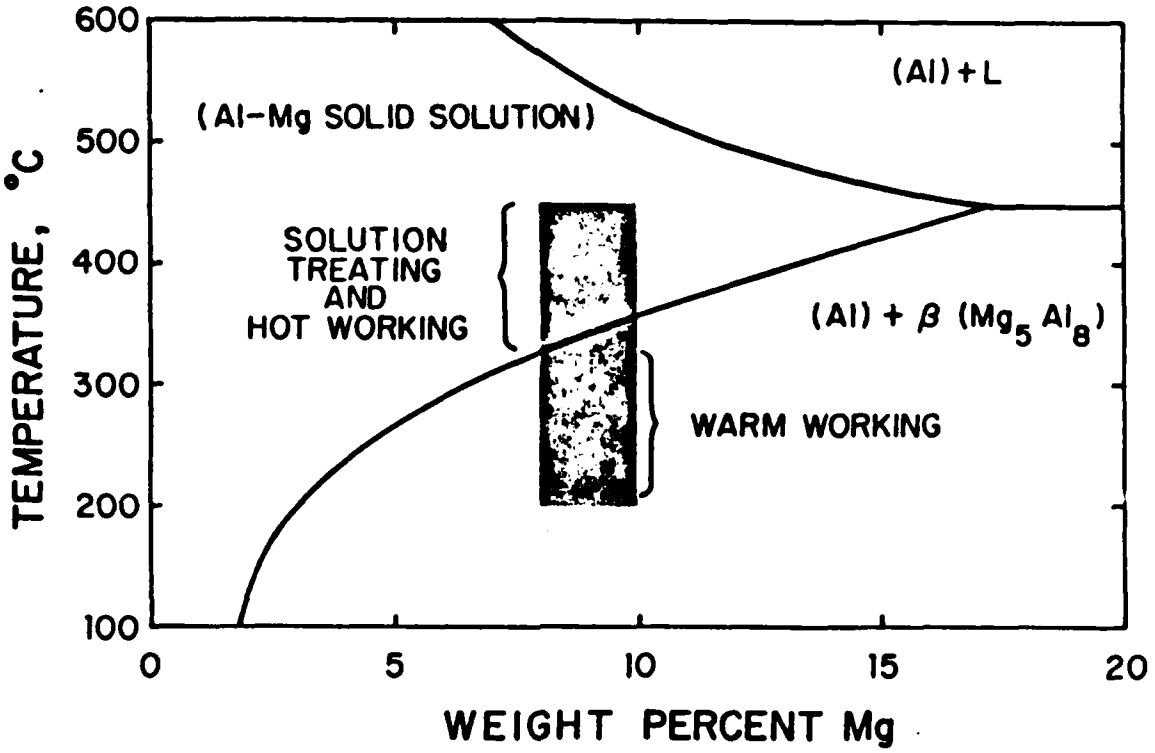

Figure 3.2. Portion of the Al-Mg Phase Diagram Showing Where Material Processing was Done.

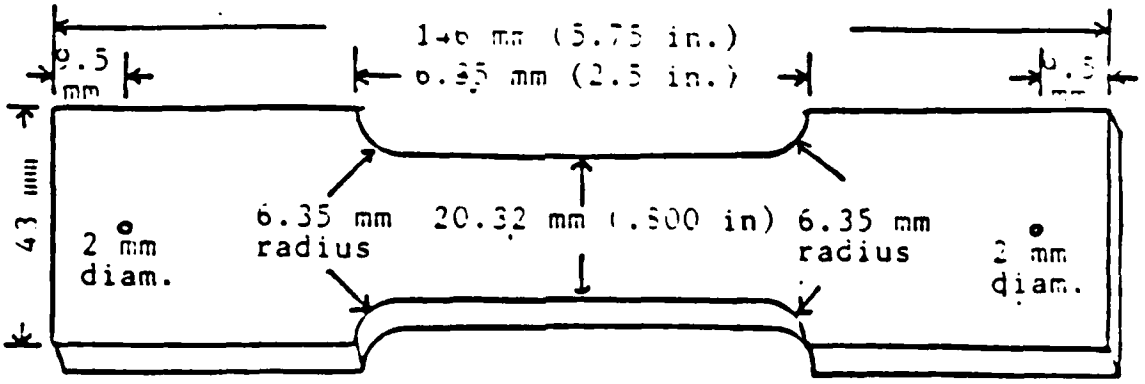

Figure 3.3. Superplastic Deformation Specimen Geometry

(0.80in) length. These dimensions gave a gage width-to-length ratio of 1 to 4. Figure 3.4 shows the geometry of this small room temperature specimen. Also, due to the non-uniform thickness of the gage length section after the deformation, a portion of the small room temperature test specimens were milled to uniform thickness.

In addition, to investigate further the superplastic response at warm temperature, two blanks were cut from the rolled sheets. The dimensions of those blanks were 63.5 mm (2.500 in) in length by 12.7 mm (0.500 in) in width. These were machined to give nominal gage dimensions of 5.1 mm (0.200 in) width and 12.7 mm (0.500 in) length. This results in a gage width-to-length ratio of the 1 to 2.5. Shoulder radius for these specimens was 1.59 mm (0.0625 in). Figure 3.5 shows this geometry. This geometry is the same as used by Alcamo [Ref.18] at elevated temperatures to provide a better-defined gage section. Specimens for ambient temperature testing were also cut from the rolled sheets and were machined to the dimensions presented by Klankowski [Ref.21, p.27] for room temperature test specimens. This geometry was also used by Grider [Ref.22]. Figure 3.6 shows this specimen geometry.

Special attention was given to ensure blanks were cut with long axis parallel to the rolling direction and any stress concentrations or burrs were removed. This was done

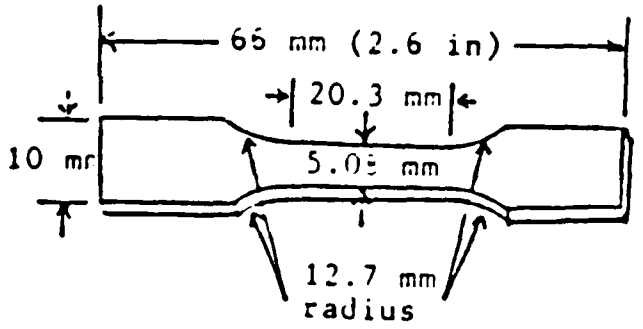

Figure 3.4. Small Room Temperature Test Specimen.

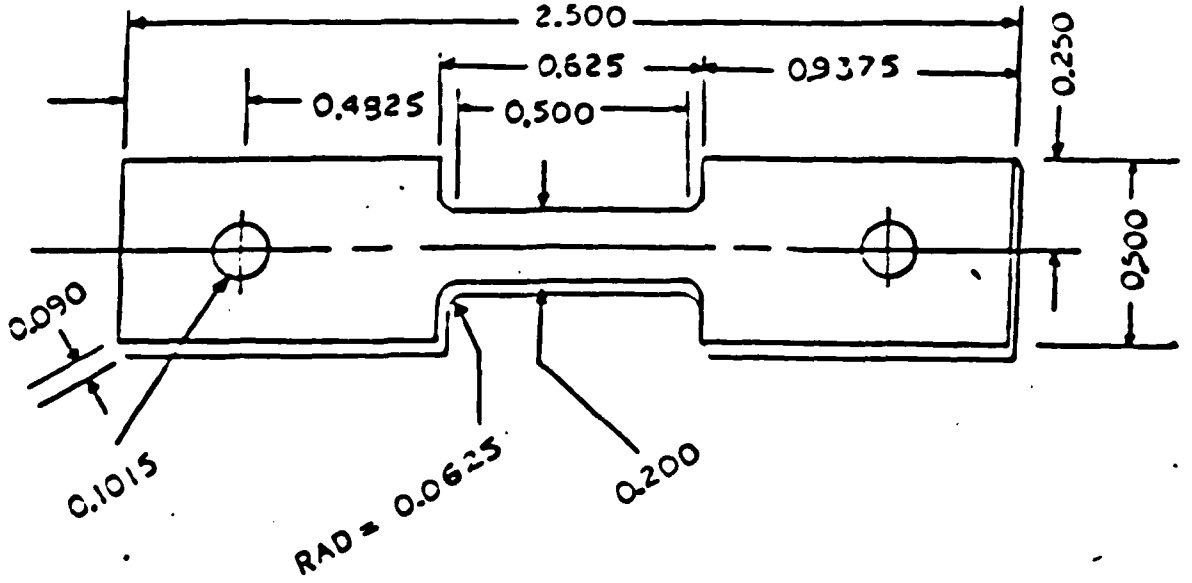

Figure 3.5. Tensile Test Specimen Geometry.

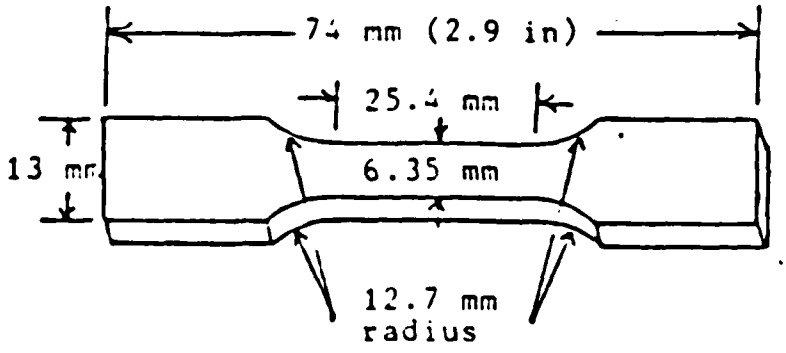

Figure 3.6. Standard Room Temperature Test Specimen.

out of concern for possible notch sensitivity resulting from processing.

E. SPECIMEN TESTING

Simulated superplastic forming was conducted on an electromechanical Instron machine and was done at 300°C and at strain rates of either 1.7×10^{-3} s^{-1} or 1.7×10^{-2} s^{-1}. Crosshead speeds for these rates were 5.08 mm/min (0.2 in/min) or 50.8 mm/min (2 in/min). Specimens were placed in wedge grips and held in place by pins passing through the wedges. The wedges were placed into grip assemblies which were screw mounted on pull rods connected to the Instron machine. The wedges, grips and pull rods were machined from type 304 stainless steel. To maintain a constant specimen temperature during testing, a Marshall Model 2232 three-zone clamshell furnace containing three vertical oriented heating elements was used. The heating elements were individually regulated by three separate controllers, each using its own thermocouple sensor located adjacent to the element. The furnace was insulated by placing thin strips of fiber insulation between the mating faces of the clamshell. Fiberglass insulation pads were wrapped around each pull rod near the top and bottom of the furnace. When the furnace was closed, an additional thick glass fiber insulation was fitted around the pull rods outside the furnace to minimize the flue effects.

Four thermocouples were placed inside the furnace to monitor the specimen temperature. Two thermocouples were brought in along each pull rod and were secured to the pull rod with Nichrome wire. One thermocouple from each end was placed in contact with the end tab of the specimen to monitor directly its temperature. The other thermocouple from each end was placed near, but not touching, the gage section of the specimen. Those two thermocouple along the gage section were placed on opposite sides of the gage section and overlapped by about one inch before deformation, to facilitate good gage section temperature monitoring during the nominal two to four inches of deformation given to the samples. The furnace controllers were adjusted so that the four thermocouples were all within 1% of 300°C. The furnace, grips and pull rods were heated for 24 hours before a series of tests to give the components time to reach thermal equilibrium. After a sample was mounted, the furnace was closed and the four thermocouples were monitored until they were back within 1% of 300°C. This would usually take about one hour and then deformation would begin.

Ambient temperature testing was conducted on the same electromechanical Instron machine. A crosshead speed of 1.27 mm/min (0.05 in/min) was used for all ambient temperature testing. This resulted in a strain rate of $8.3 \times 10^{-4}\ S^{-1}$ for the 1 inch gage length specimens and a strain rate of $1.04 \times 10^{-3}\ S^{-1}$ for the 0.8 inch gage length

specimens. Specimens were mounted in vise action grips. Standard room temperature specimens tested were in the as-rolled condition and also annealed at 300°C for 0.5, 1 and 5 hours. The Instron machine was calibrated before each series of tests.

F. DATA REDUCTION

Elongation was computed by measuring the distance L between the scribed gage marks after deformation or fracture using the equation 3.1:

$$\% \text{ Elongation} = \frac{(L - Lo)}{Lo} \times 100 \qquad \text{(eqn 3.1)}$$

where Lo was the gage length before pulling depending on the size of specimen tested. The Instron machine strip-chart recorded the applied load (lbs) vs chart motion. The magnification ratio between chart speed and crosshead speed was 100 for the ambient temperature testing and 10 for the elevated temperature testing.

From the strip chart, raw data points of chart displacement and load were taken from the curve. A "floating slope" was used on the strip chart from which measurements were taken. This was used to remove such variables as grip adjustment and elasticity of the sample as well as Instron components themselves. There was routinely a discrepancy between the strain determined from the strip chart and that measured from the gage marks. This was

attributed to deformation outside of the scribe marks, grip seating, tension rod alignment and other variables. In order to predict as accurately as possible the true elongations from the chart values, a scale factor equal to the ratio of the measured elongation at fracture to the chart-predicted value at fracture was applied to each data point of a given test and hence at fracture the two values coincide exactly.

This input data was analyzed by using a Basic computer program, provided in the Appendix, which was run on an IBM XT compatible computer and the following basic formulas:

$$S = P/Ao \quad \text{(Engineering Stress)} \quad \text{(eqn 3.2)}$$

$$e = (L - Lo)/Lo \quad \text{(Engineering Strain)} \quad \text{(eqn 3.3)}$$

$$\sigma = S(1 + e) \quad \text{(True Stress)} \quad \text{(eqn 3.4)}$$

$$\varepsilon = \ln(1 + e) \quad \text{(True Strain)} \quad \text{(eqn 3.5)}$$

This reduced data was then sent to the IBM 3033 computer for further generation of graphics using the Easyplot routine.

G. METALLOGRAPHY

In support of this research, optical microscopy, scanning electron microscopy (SEM) and transmission electron microscopy (TEM) were carried out following standard

metallographic techniques. [Ref. 37] Specimens for scanning electron microscopy were attached to standard stubs with conductive silver paste. Specimens examined by light microscopy were first cold-mounted in a cylindrical plastic medium by an acrylic compound. Mounted specimens were then polished by wet silicon carbide abrasive paper following a sequence of 240, 320, 400, and 600 grit papers. This process took about 30 minutes. An ultrasonic cleaning was given to remove any embedded abrasive particles before the next step of polishing. Then a rough polish was given on 600 grit alumina (Al_2O_3) powder in distilled water using billiard cloth fixed to a wheel rotating at 350 RPM. Considerable hand pressure was used initially and then gradually reduced. This process took 5 to 7 minutes maximum to complete. Again an ultrasonic cleaning was necessary. The final polishing was accomplished with an eleven micron magnesium oxide powder (MgO) in distilled water on a wheel rotating at 350 RPM. A moderate to light hand pressure was used and the process took about 5 minutes. A final ultrasonic cleaning was necessary too. Following this, the specimens were electrolytically polished to remove the final traces of mechanical disturbance from the surface. The specimens were submerged in a solution of 20% HNO_3 in methanol and connected as the anode across a constant 10 vdc potential. Liquid nitrogen was used to reduce the temperature of the electrolyte to 0°C, thereby slowing the

reaction to manageable times. Polishing times varied from 5-10 seconds depending upon the degree of warm working received. Following electrolytic polishing, the specimens were anodically etched. The electrolyte employed was composed of 34.6 ml of HF acid, 13.6 gm of HBO_3 acid and sufficient distilled water to make up a solution of 1000 ml volume. The specimens were submerged, connected anodically across a 10 vdc potential and etched for about 5 seconds, the time again depending upon degree of warm working. Optical microscopy was conducted with a Zeiss ICM-405 optical microscope.

For transmission electron microscopy blanks of 50 μm thickness were sectioned parallel to the rolling plane of the superplastically deformed specimens. By mechanical grinding on fine-grit silicon carbide paper, the thickness was reduced to 35 μm. The final thickness of 25-30 μm was achieved by caustic etching at 60°C in NaOH. A final surface cleaning in a solution of 30% HNO_3 in methanol was given to each blank. Thin foil specimens of 3 mm disk size were prepared with a Struers polisher utilizing 20% HNO_3 in methanol as the electrolyte. The electrolyte temperature was reduced to -20°C and a potential of 15 vdc was applied. Thin foil specimens were examined in a JEOL (JEM-100 CX 11) transmission electron microscope.

IV. RESULTS AND DISCUSSION

A. THERMOMECHANICAL PROCESSING CONDITIONS

1. As-Cast Material

The Al-10%Mg-0.1%Zr alloy used in this study was produced by the direct chill casting method. As described by Berthold [Ref. 19, p.35], this method provides a relatively high cooling rate which is necessary to reduce coring and segregation in the alloy. Optical micrographs of the as-cast material showed that the microstructure is dendritic and thus non-homogeneous. The β precipitate (Mg_5Al_8) is heavily concentrated at the grain boundaries, with very little in grain interiors. Also, constituent particles of square shape, located in the centers of many grains, were identified as $ZrAl_3$ particles which suggests that this phase ($ZrAl_3$) forms as a primary phase and serves further as nucleation sites for the Al solid solution.

2. Solution-Treatment Conditions

Solution treatment of the alloy was done at 440°C for 40 hours to obtain a single-phase solid solution. This temperature of solution treatment was selected based on previous work of Klankowski [Ref. 21], which showed that there is no discernable improvement in distribution of the Zr or enhancement of the room temperature mechanical properties of the alloy, to be gained by solution treating at a higher temperature of 490°C.

3. Upset-Forged Conditions

In this work hot working was done by isothermal upset-forging at 440°C after the 40 hours of solution treatment. This working was intended to further refine and homogenize the cast microstructure. Each billet was given a reduction of approximately 73%, equivalent to a true strain of 1.3 in upset-forging. The billets were then annealed for one hour at the solution treatment temperature prior to oil quenching to ensure a quenching temperature from above the solvus.

In this work, hot working was done at 440°C since previous work by Becker [Ref. 14] and Grider [Ref. 22] indicated that the structure resulting from working at higher temperature is coarser. This is also noted by Dieter [Ref. 34, p. 560] and it was also reported by Wise [Ref. 35] who encountered hot shortness when using a higher temperature of 480°C for some samples.

4. Warm-Rolled Conditions

As reported in previous work [Ref. 22], the lightrolling reduction scheme resulted in non-uniform working of the material. The layers near the surface of the rolled sheet had been more extensively worked than the center. Because of this, residual stresses will be developed along with possible edge cracking, as discussed by Dieter [Ref. 34]. Those residual stresses, combined with inverse segregation noted in the as-cast ingot, appear to be

important in edge cracking. Subsequently, a change was made in the processing. A heavy reduction scheme was introduced by increasing the reduction per pass from 1.0 mm (0.04 in) to 2.0 mm (0.08 in); it was observed that the edge defect was eliminated. In addition, by rolling with lesser time between passes, i.e., allowing less recovery time, the microstructure should have a net increase in dislocation density and lessened recovery. Wert [Ref. 23] reports that if heavy deformation is not used, then the original elongated grains are not sufficiently distorted and discontinuous recrystallization does not produce an equiaxed microstructure needed to enhance superplastic properties in processing of high strength, i.e., 7xxx alloys.

In this work, a still-heavier rolling reduction scheme was used by taking a 2.5 mm reduction per pass, anticipating a stranger and possibly more ductile material as well. Figure 4.1 shows the microstructure of material experiencing this heavier rolling reduction, which seems to be finer but more banded compared with previous processing seems.

Table II shows in summary the thermomechanical processing conditions of previous and present work.

B. MECHANICAL TESTING

1. Ambient Temperature Testing.

As-rolled and as-rolled plus statically annealed specimens were tested at $8.3 \times 10^{-4}\ S^{-1}$ strain rate, and

Figure 4.1. Optical micrograph of an Al-10%Mg-0.1%Zr alloy, warm rolled at 300°C to a true strain of 2.5 (92%), in the longitudinal orientation. 200X.

TABLE II

THERMO MECHANICAL PROCESSING CONDITIONS OF PRESENT AND PREVIOUS WORK

	SOLUTION TREATMENT	UPSET FORGING			WARM ROLLING			
	TIME-TEMP	t_f	REDUCTION	TRUE STRAIN	TYPE	t_f	REDUCTION	TRUE STRAIN
(1)	24HRS-440°C OR 24HRS-480°C	1.15"	70%	1.2	LIGHT REDUCTION 6-10 MIN/PASS 1 MM/PASS	0.15"	83%	1.8
(2)	5HRS-400°C AND 19HRS-480°C	1"	73%	1.3	LIGHT REDUCTION 6-10 MIN/PASS 1 MM/PASS	0.15"	89%	2.2
		0.8"	78%	1.5	HEAVY REDUCTION 4 MIN/PASS 2 MM/PASS	0.12"	85%	1.9
(3)	40HRS-440°C	1"	73%	1.3	HEAVY REDUCTION 4 MIN/PASS 2.5 MM/PASS	0.09"	92%	2.5

(1) Klankowski [Ref. 21]
(2) Grider [Ref. 22]
(3) This Work

ambient temperature. Static annealing was done at the warm forming temperature of 300°C for 0.5, 1, and 5 hours to provide data for comparison with previous work by Grider [Ref. 22] and Klankowski [Ref. 21]. Data provided in Table III shows that the as-rolled ductility is approximately 10.5 percent. After one hour of annealing at 300°C, the ductility reaches 13 percent. Although annealing time was increased to 5 hours, ductility remained almost constant. Yield strength is approximately 51.4 KPSI (354 MPA) and ultimate tensile strength 80.9 KPSI (588 MPa) for the as-rolled material. After one hour of annealing yield strength and ultimate strength decreased to approximately 35 KPSI (241 MPa) and 58 KPSI (400 MPa), respectively, and stayed almost constant for annealing time increasing to 5 hours. Table IV shows averaged data from ambient temperature mechanical test of Al-10%Mg-0.1%Zr alloy in the as-rolled condition and for various annealing times at 300°C for previous work by Grider [Ref. 22, p.50] and also this work. Figure 4.2 is a graphical representation of data shown in Table IV, from which it is clear that going to a greater true rolling strain, from ±2 in previous work to 2.5 in this work, results in a stronger but less ductile material. Figure 4.3 shows engineering stress versus engineering strain curves which compare typical data for the heavy rolled material of previous work (true strain ±2) and this work (true strain 2.5).

TABLE III

AMBIENT TEMPERATURE MECHANICAL TEST DATA OF AL-10%MG-0.1%ZR ALLOY IN THE AS-ROLLED CONDITION (HEAVY REDUCTION PROCESSING) AND FOR ANNEALING TIMES AT 300°C

TIME ANNEAL AT 300°C (HRS)	σ_y (KPSI)	σ_y (MPA)	σ_u (KSPI)	σ_u (MPS)	DUCTILITY (%ELONGATION)
0	47.9	330.3	81.0	558.5	12.5
0	58.8	405.4	82.0	565.4	9.1
0	57.4	395.8	79.7	549.5	8.4
0	48.0	331.0	78.0	537.8	11.7
0	45.0	310.3	83.7	577.1	11.4
0.5	37.9	261.3	69.0	475.7	12.0
0.5	35.9	247.5	69.7	480.6	13.2
0.5	34.0	234.4	69.5	479.2	13.1
0.5	36.3	250.3	69.4	478.5	13.0
0.5	35.4	244.1	68.3	470.9	12.7
1.0	35.8	246.8	67.7	466.8	12.3
1.0	34.5	237.9	67.3	464.0	13.0
1.0	27.2	187.5	69.0	475.7	13.9
1.0	35.3	243.4	67.5	465.4	12.7
1.0	35.7	246.1	68.0	468.8	12.5
5.0	23.5	162.0	65.6	452.3	14.0
5.0	33.5	231.0	64.6	445.4	13.0
5.0	33.4	230.3	66.7	459.9	12.9
5.0	34.3	236.5	66.0	455.0	12.6
5.0	28.2	194.4	64.6	445.4	12.9

TABLE IV

AMBIENT TEMPERATURE MECHANICAL TEST AVERAGED DATA OF AL-10%MG-0.1%ZR ALLOY IN THE AS-ROLLED CONDITION (HEAVY REDUCTION PROCESSING) AND FOR VARIOUS ANNEALING TIMES AT 300°.

TIME ANNEAL AT 300°C (HRS)	σ_y (KPSI)		σ_u (KPSI)		(% ELONGATION)	
	GRIDER(1)	SOLOMOS(2)	GRIDER(1)	SOLOMOS(2)	GRIDER(1)	SOLOMOS(2)
0	51.1	51.4	67.2	80.9	18.8	10.6
1.0	36.8	35.3	58.9	67.9	16.5	12.9
5.0	32.5	32.4	56.7	65.5	18.5	13.1

(1) Grider [Ref. 22, p.50]
(2) This work

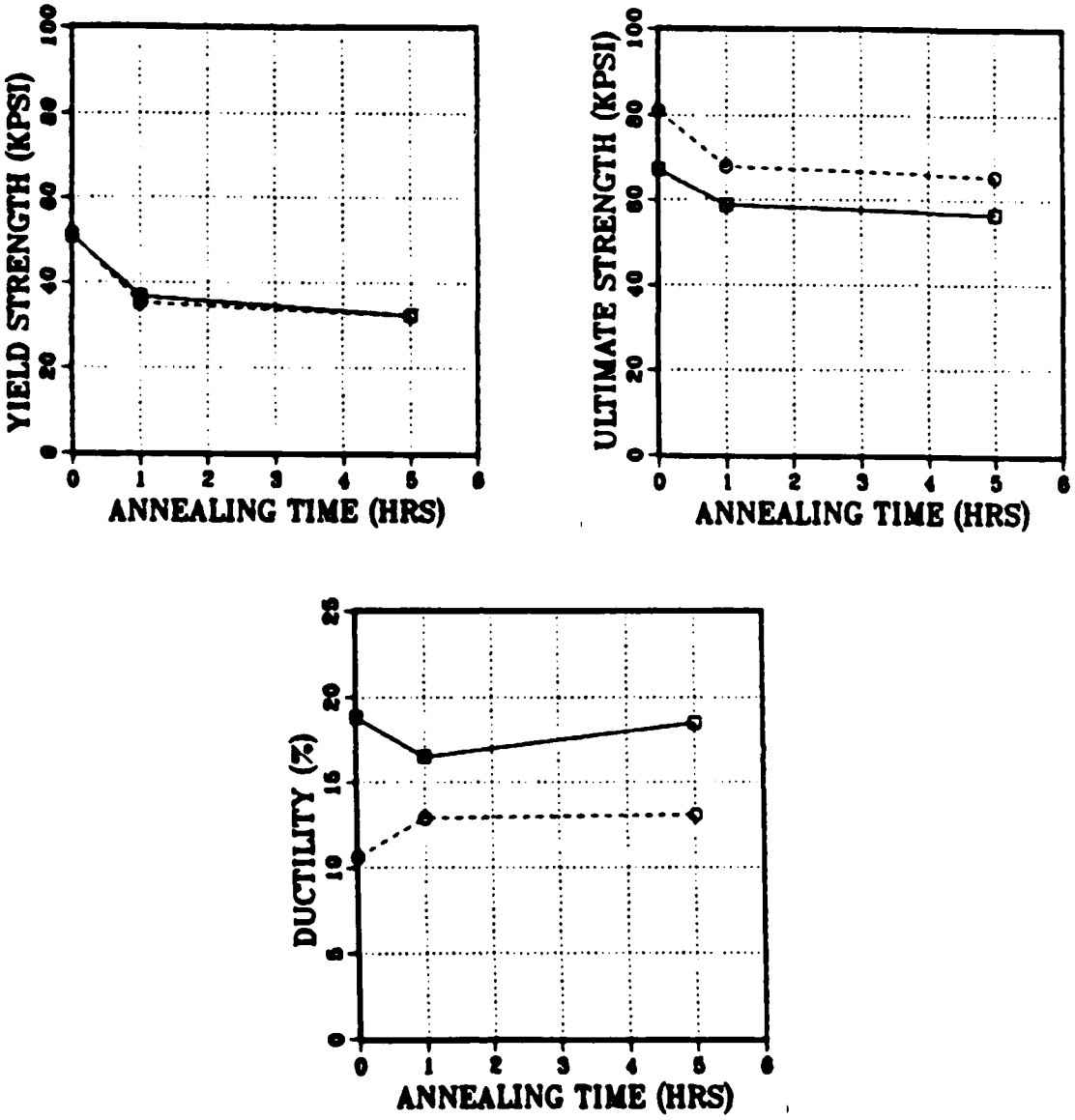

Figure 4.2. Results of ambient temperature tension testing of heavy reduction processed material; true strain ≈2, solid line, from Grider [Ref. 22]; true strain 2.5, dash line, this work.

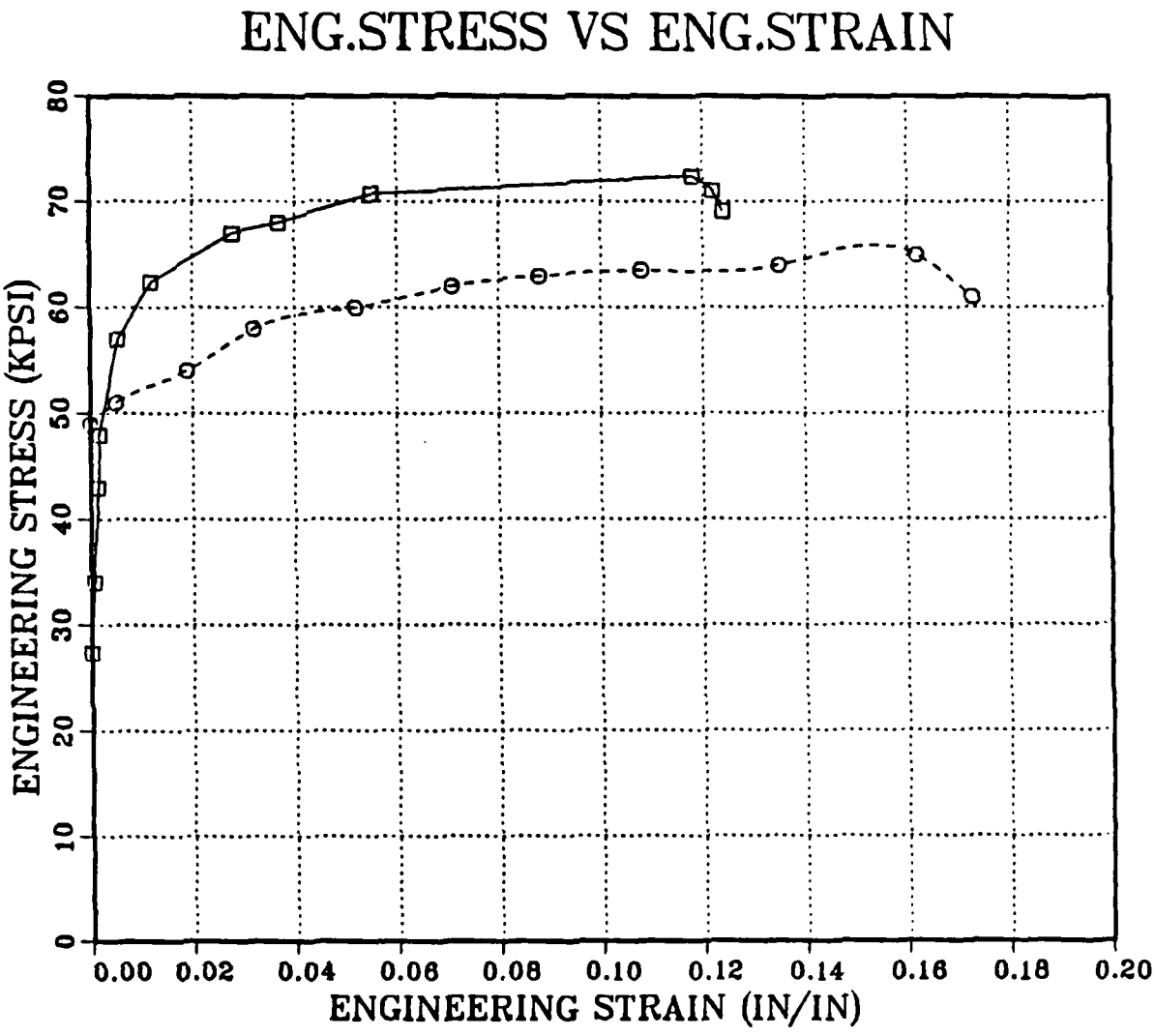

Figure 4.3. Engineering stress versus engineering strain for an ambient temperature tension test on as-rolled material showing the influence of the rolling strain: true strain ≈2, dashed line, from Grider [Ref. 22]; true strain 2.5, solid line, this work.

2. Elevated Temperature Testing

a. Simulated Superplastic Forming at 300°C

For the simulated superplastic forming, eleven samples of the as-rolled material were machined to the specimen geometry shown in Figure 3.3 and were deformed at 300°C. The initial schedule called for three samples to be deformed to 100% strain at 1.67×10^{-2} S^{1} strain rate, four to be deformed to 100% strain at 1.67×10^{-3} S^{1} strain rate and four to be deformed to 200% strain at 1.67×10^{-3} S^{1} strain rate. Even though in the first test conducted the specimens failed before reaching the strain anticipated, it was decided to continue the test series. True stress versus true strain data are shown in Figure 4.4, mechanical test data are provided in Table V and it can been seen that the simulated superplastic forming was not successful in that less strain was obtained than anticipated based on previous data and on the idea that the heavier working scheme would enhance the ductility by resulting in a finer continuously recrystallized grain size. On the other hand, the ductility achieved is consistent with that reported by Wise [Ref. 35] and unpublished work of Salama and not, therefore, an anomaly of this research alone. In general, the material worked by the heavy reduction scheme is not as highly ductile. Transmission electron microscopy conducted at this point showed that the material possesses a very fine

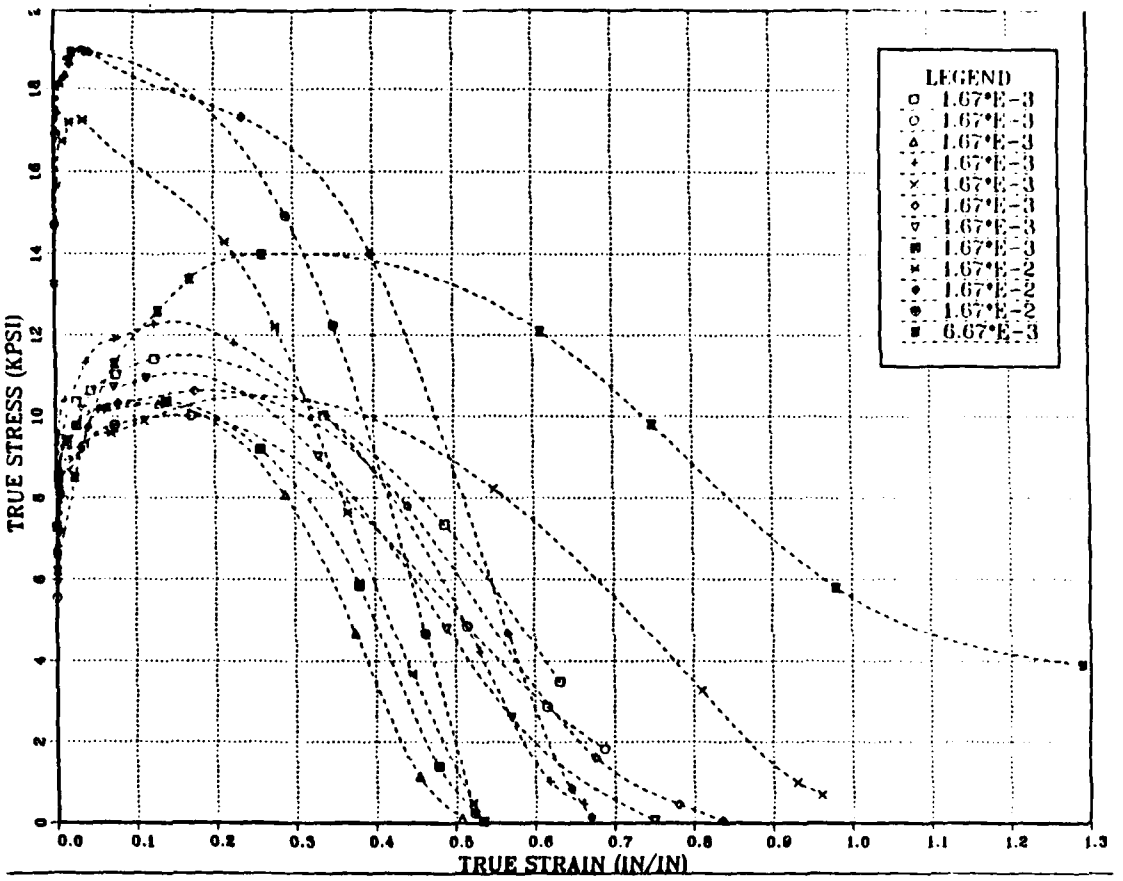

Figure 4.4. True stress versus true strain data for elevated temperature tension testing,conducted at 300°C for the heavy reduction processing material, at 1.67 X 10^{-3} S^{-1}, 1.67 X 10^{-2} S^{-1} and 6.67 X 10^{-3} S^{-1} strain rate.

TABLE V

ELEVATED TEMPERATURE MECHANICAL TEST DATA FOR THE Al-10%Mg-0.1%Zr ALLOY, TESTED AT 300°C

SPECIMEN I.D.	(SEC^{-1})	(KSPI)	(MPA)	(% ELONGATION)
S1a (1)	1.67×10^{-3}	11.3	78.0	98.8
S1b (2)	1.67×10^{-3}	9.9	68.5	118.2
S1c (3)	1.67×10^{-3}	10.4	71.5	66.0
S1d (4)	1.67×10^{-3}	12.2	84.0	110.0
S2a (5)	1.67×10^{-3}	9.9	68.2	161.0
S2b (6)	1.67×10^{-3}	10.6	73.1	130.0
S2c (9)	1.67×10^{-3}	10.9	75.4	112.5
S2d (8)	1.67×10^{-3}	10.4	71.7	70.0
S3a (9)	1.67×10^{-2}	17.0	117.2	68.5
S3b (10)	1.67×10^{-2}	19.0	131.0	95.0
S3c (11)	1.67×10^{-2}	18.8	129.3	68.5
ST1 (12)	6.67×10^{-3}	12.1	83.7	262.0

S1, S2, S3 Specimen's geometry shown in Figure 3.3
ST1 Specimen's geometry shown in Figure 3.5

structure. Figure 4.5 and 4.6 show micrographs of the gage and grip sections of one of the simulated superplastic warm deformed specimen where the fine structure is clear. It is not known, however, the extent to which the material is continuously recrystallized. Specifically, it is not known if it meets the grain boundary structure requirements in all details, that is, the misorientations were not determined to assess the completeness of the microstructure evolution from a subgrain to a grain structure. The microstructure is very fine and therefore it was decided to go ahead and complete the schedule that was set up.

b. Stress-Strain Rate Data

To compare the results of this work with the results of Wise's [Ref.35] work on the same material with the same thermomechanical processing and with previous work by Grider [Ref. 22, p. 61], values of true stress at 0.1 strain were obtained for the various strain rates employed, and are provided in Table V. Figure 4.7 is a graphical representation of all those data which show that the material of this work is somewhat stronger than that of Wise [Ref. 35].

c. Ductility-Strain Rate Data

Ductility data corresponding to the data of Figure 4.7 are plotted in Figure 4.8. In addition data of

Figure 4.5. TEM micrographs of the gage section of a simulated warm temperature tested sample, deformed at 300° and 1.67 X 10^{-3} strain rate.

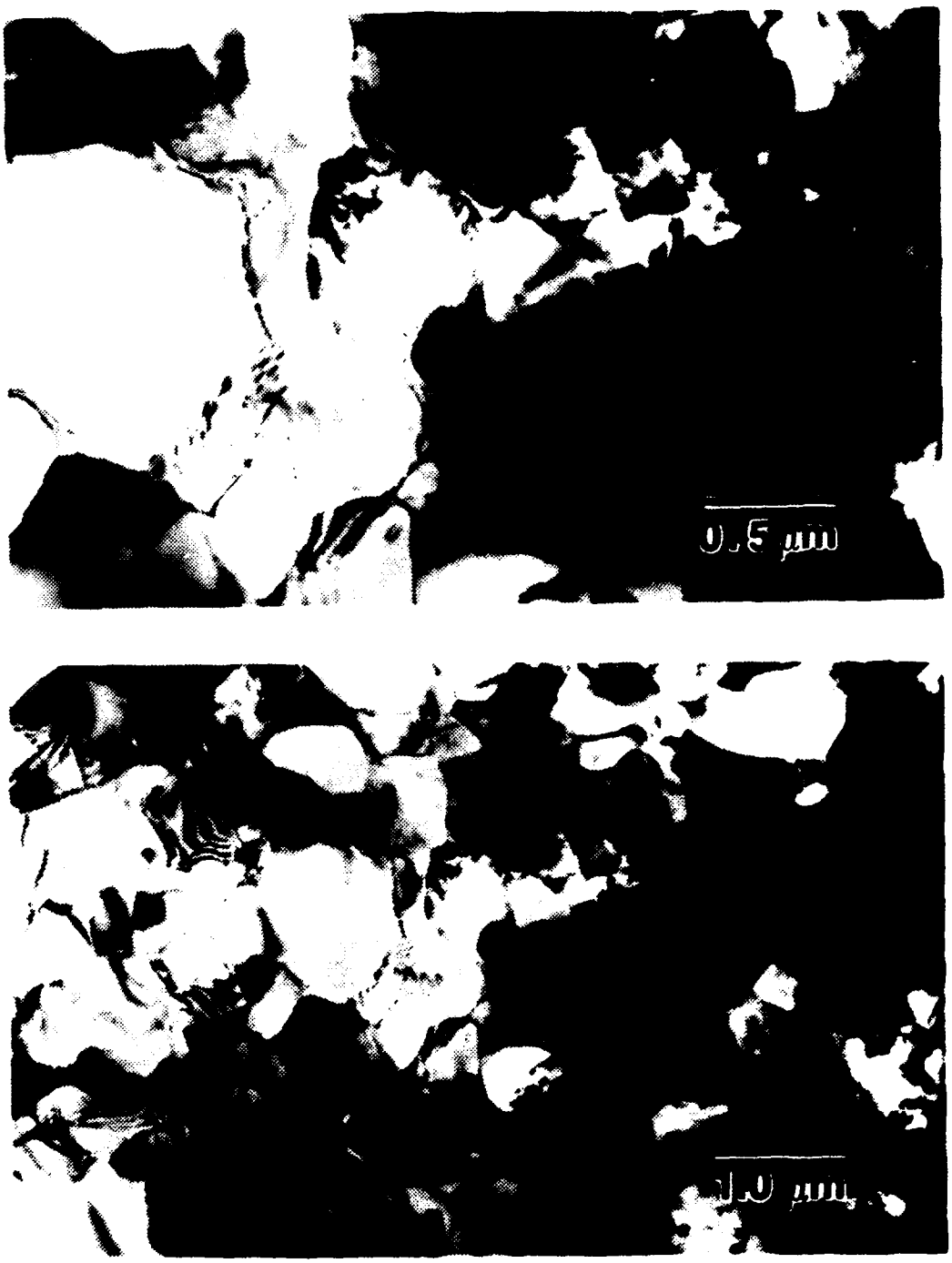

Figure 4.6. TEM micrographs of the grip section of a simulated warm temperature tested sample, deformed at 300°C and 1.67^{-3} S^{-1} strain rate.

Wise's work [Ref. 35] on two different thermomechanical processes, that is: process B, with 4% reduction per pass; 4 minutes reheat in between passes and 2.5 total strain; and process C, with 4% reduction per pass, 30 minutes reheat in between passes and also 2.5 total strain, are included. Also, data from the test of a specimen of the work, which was heated incrementally to 300°C, are plotted. Although it was expected that Grider's, this work and Wises's process A would yield the highest ductility, the peak ductility value did not exceed 264% which is very low in comparison with the 442% and 474% of processes B and C, respectively. In addition, the ductility of the specimen of this work that was incrementally heated to 300°C was no higher that 262%.

The material of this work, even though of a fine structure, still did not attain the ductility expected to result from this severe working scheme. One possibility is that what is seen in TEM is not a continuous recrystallized grain structure, but a subgrain structure instead. The true grain size would then be larger and is the reason a lesser warm temperature ductility was seen. Another possibility is that the heavy rolling scheme damages the microstructure, that is the primary $ZrAl_3$ particles documented in Klankowski work [Ref. 21, p.38] have been worked more severely, broken up and now are initiation sites for void formation internally, resulting to a lesser ductility.

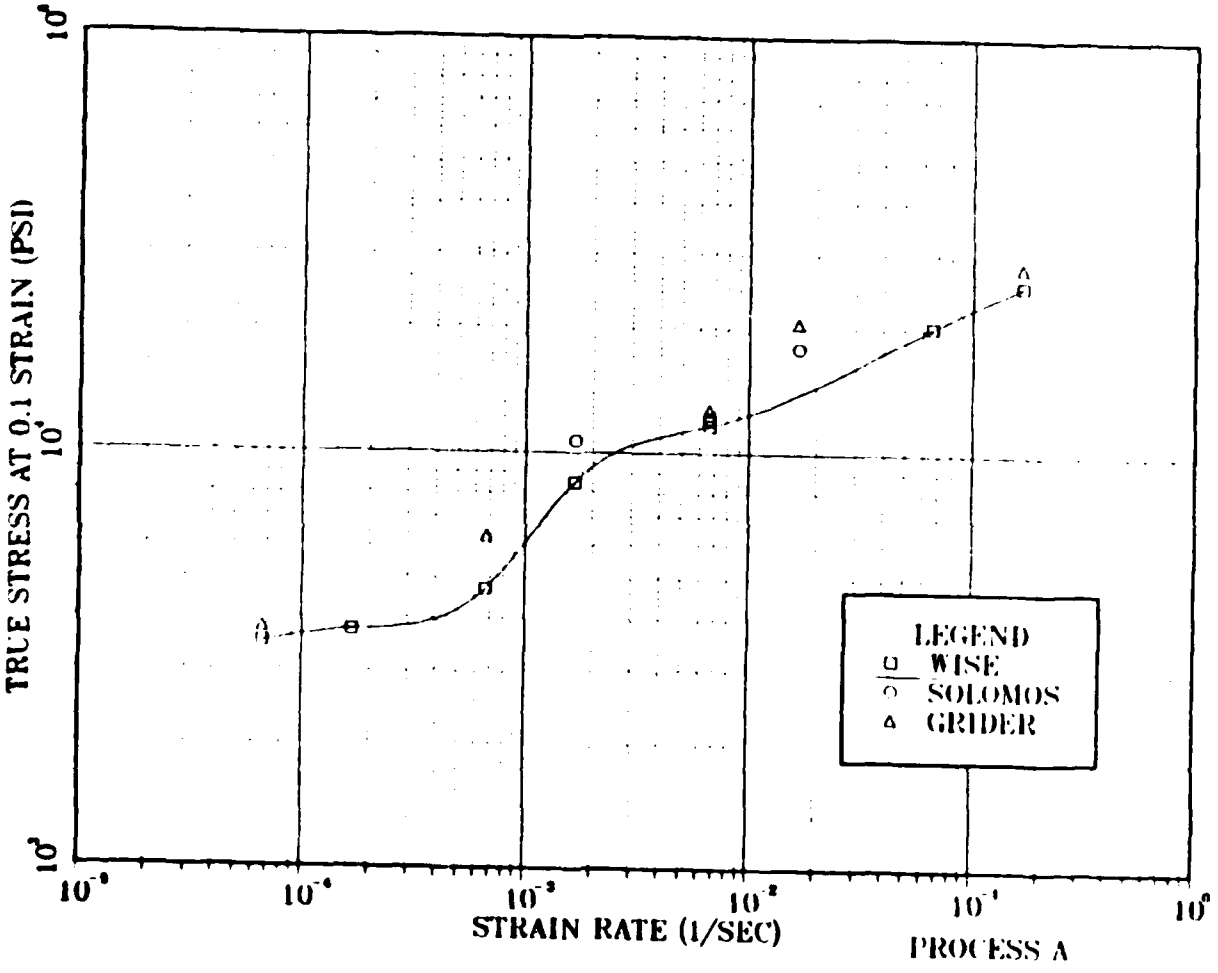

Figure 4.7. True stress at 0.1 strain versus strain rate for tension testing conducted at 300°. Comparison between previous work Grider [Ref. 22], Wise [Ref. 35] and this work.

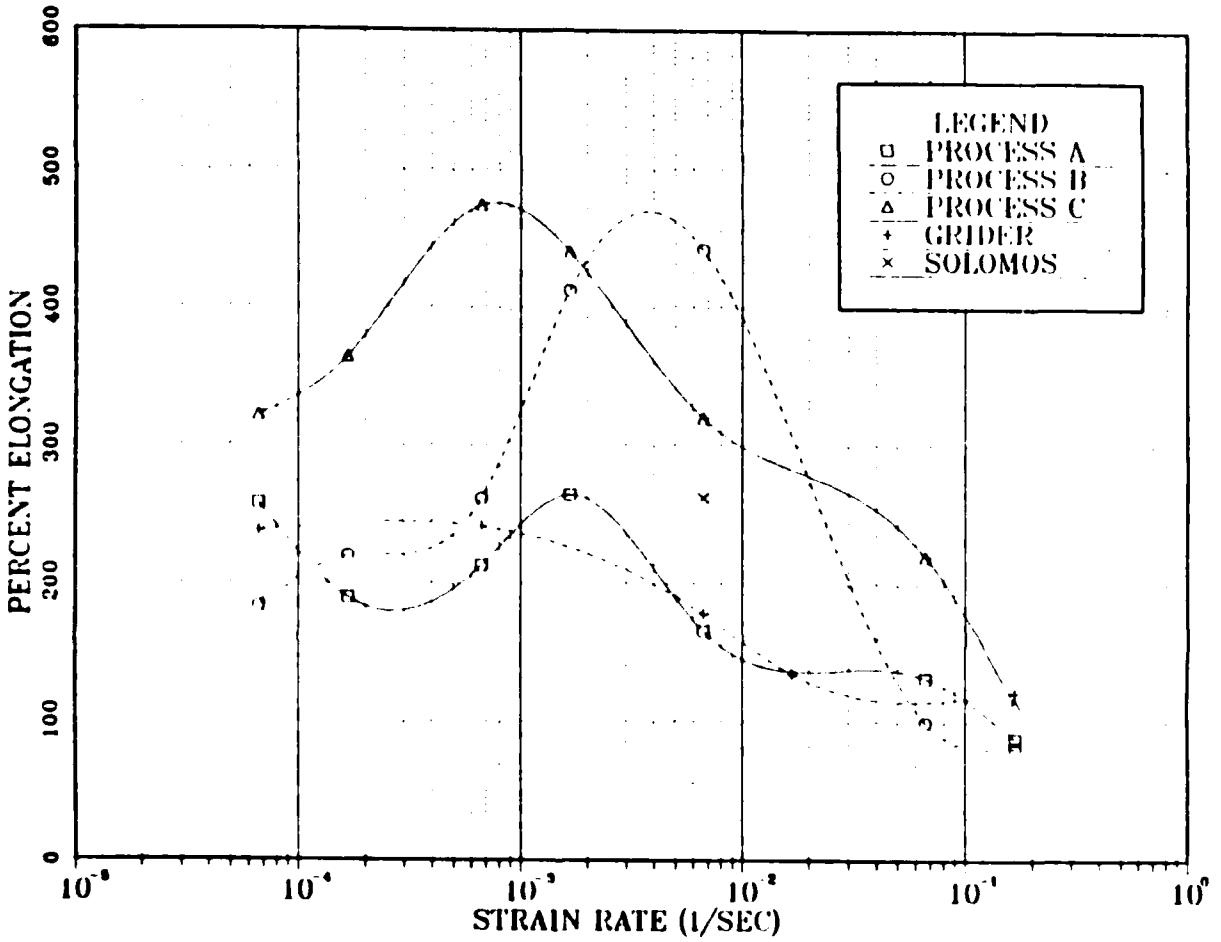

Figure 4.8. Ductility versus strain rate for tension testing conducted as 300°C. Comparison between previous work Grider [Ref. 22], Wise [Ref. 35] and this work where the specimen was heated incrementally to 300°C (50°C increments).

d. Microscopy

Basically, a fractographic microscopy investigation of the simulated warm temperature samples was set up. SEM micrographs of the fracture surface Figure 4.9 show that on the fracture surface we do see evidence for void formation, which was not seen in previous work and in Wise's work [Ref. 35]. The most high superplastic materials do not exhibit that void formation. On the lateral surface, Figure 4.10, there appear to be the grain boundaries emerging. The structure thus seems to be a continuously recrystallized structure, which suggests that the material is acting as a superplastic material. This might be saying that the primary $ZrAl_3$ particles are perhaps serving as initiation sites. Examination of the lateral surfaces was then done Figure 4.11 to see if primary particles could be identified, but none were apparent.

Tables VI, VII and Figures 4.13, 4.14 are the results of the analysis conducted on particles shown in Figure 4.12, using energy dispersive analysis. Next, samples were sectioned. In Figure 4.15, an optical micrograph after electropolishing, taken from the simulated warm deformed section of the sample, does show homogenization of the microstructure, but the $ZrAl_3$ phase is not obvious. More detailed examination was attempted on the sample of the deformed material after electroetching, but

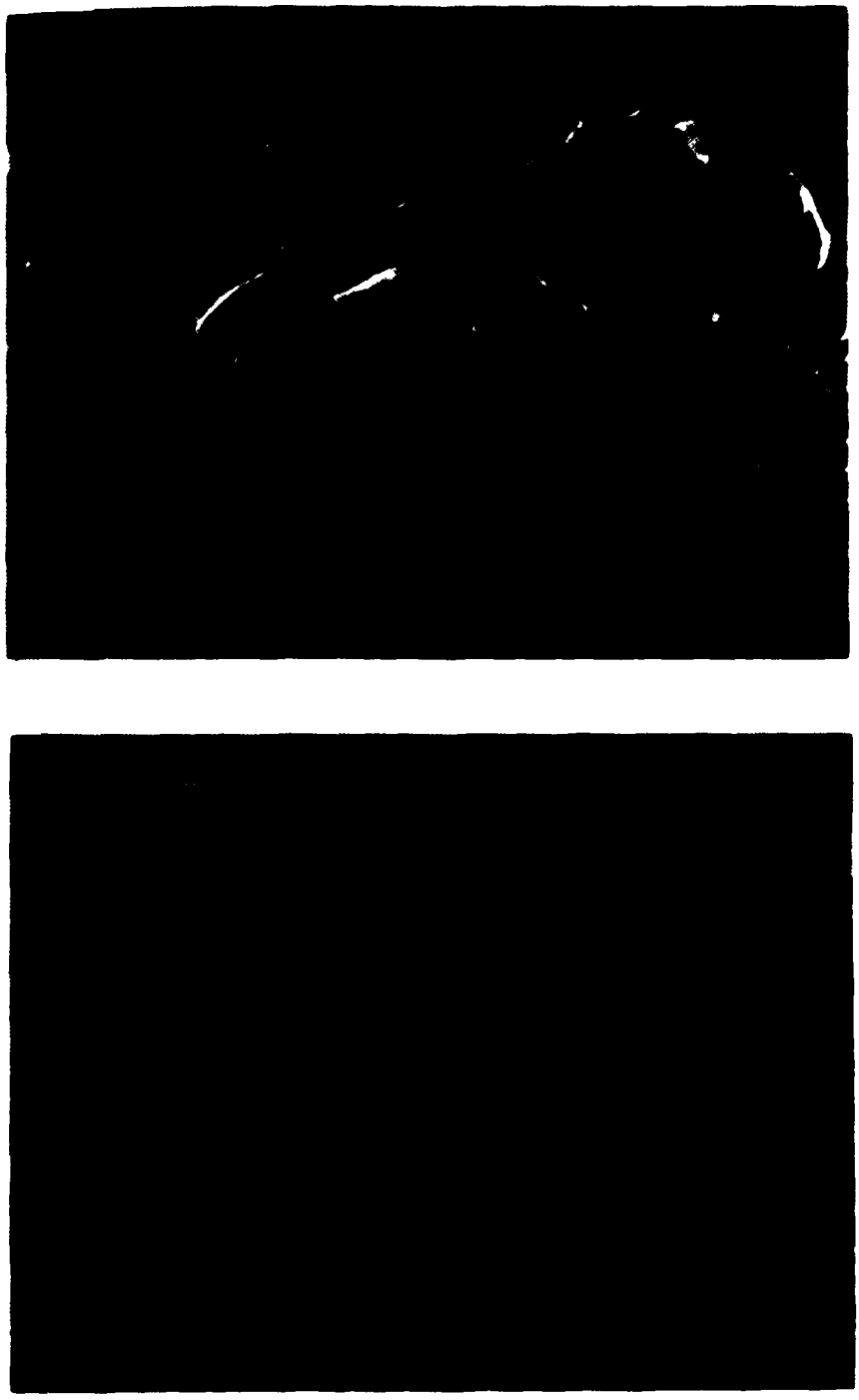

Figure 4.9. Scanning electron micrographs (SEM) of fracture surface of a simulated warm temperature tested

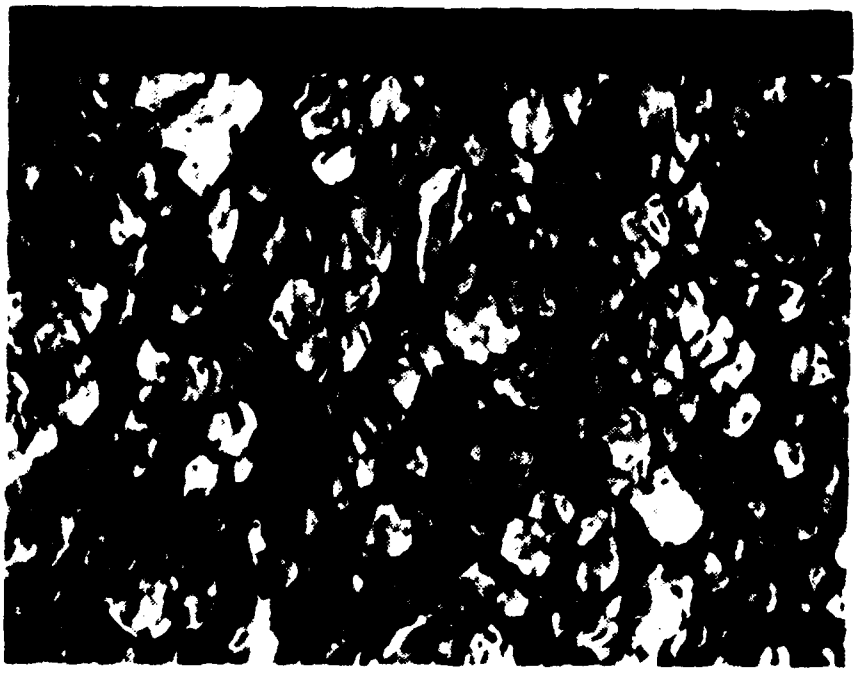

Figure 4.10. SEM micrograph of the lateral (fracture) surface of a simulated warm temperature tested sample.

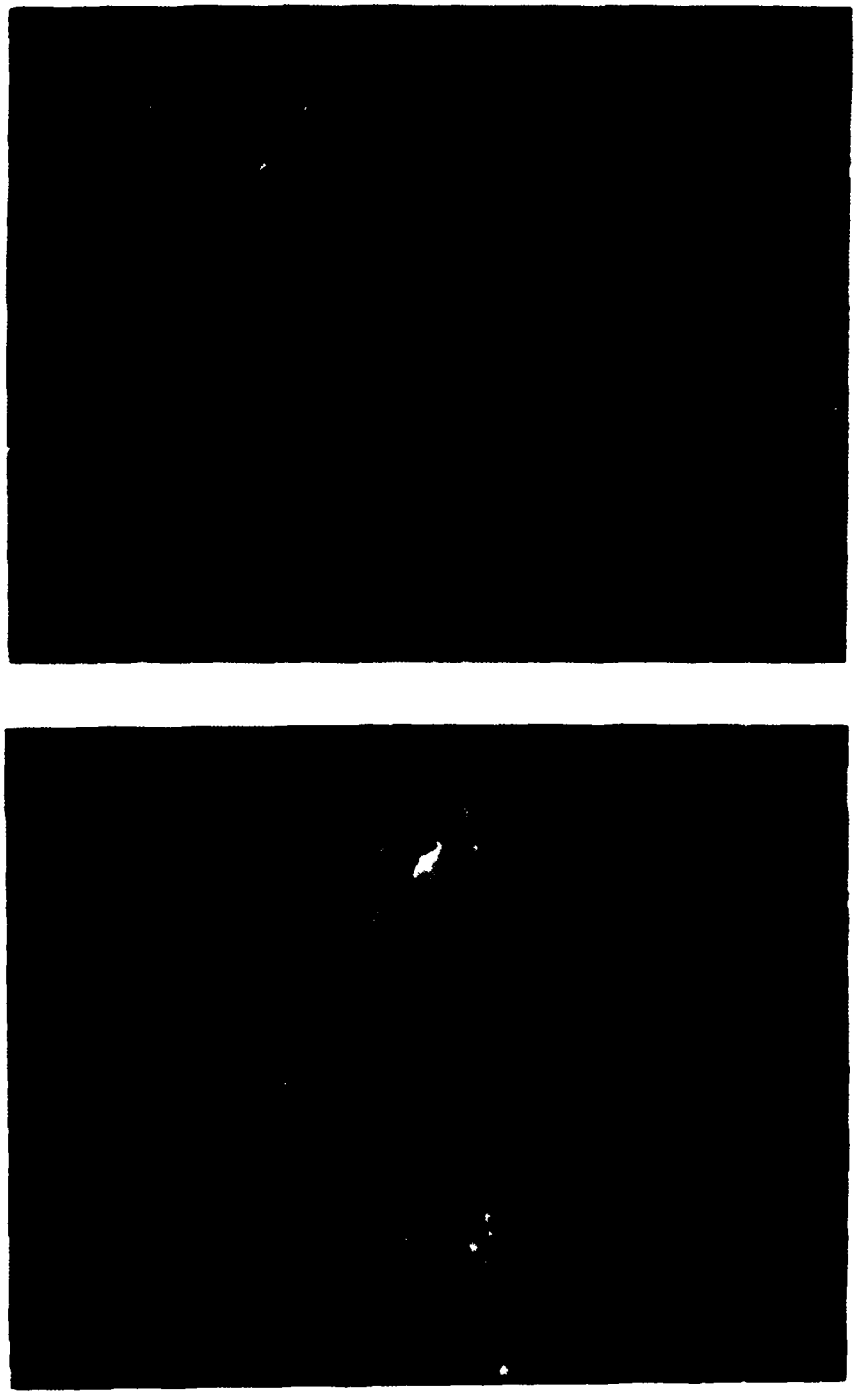

Figure 4.11. SEM micrographs of the side surfaces of a simulated warm temperature tested sample.

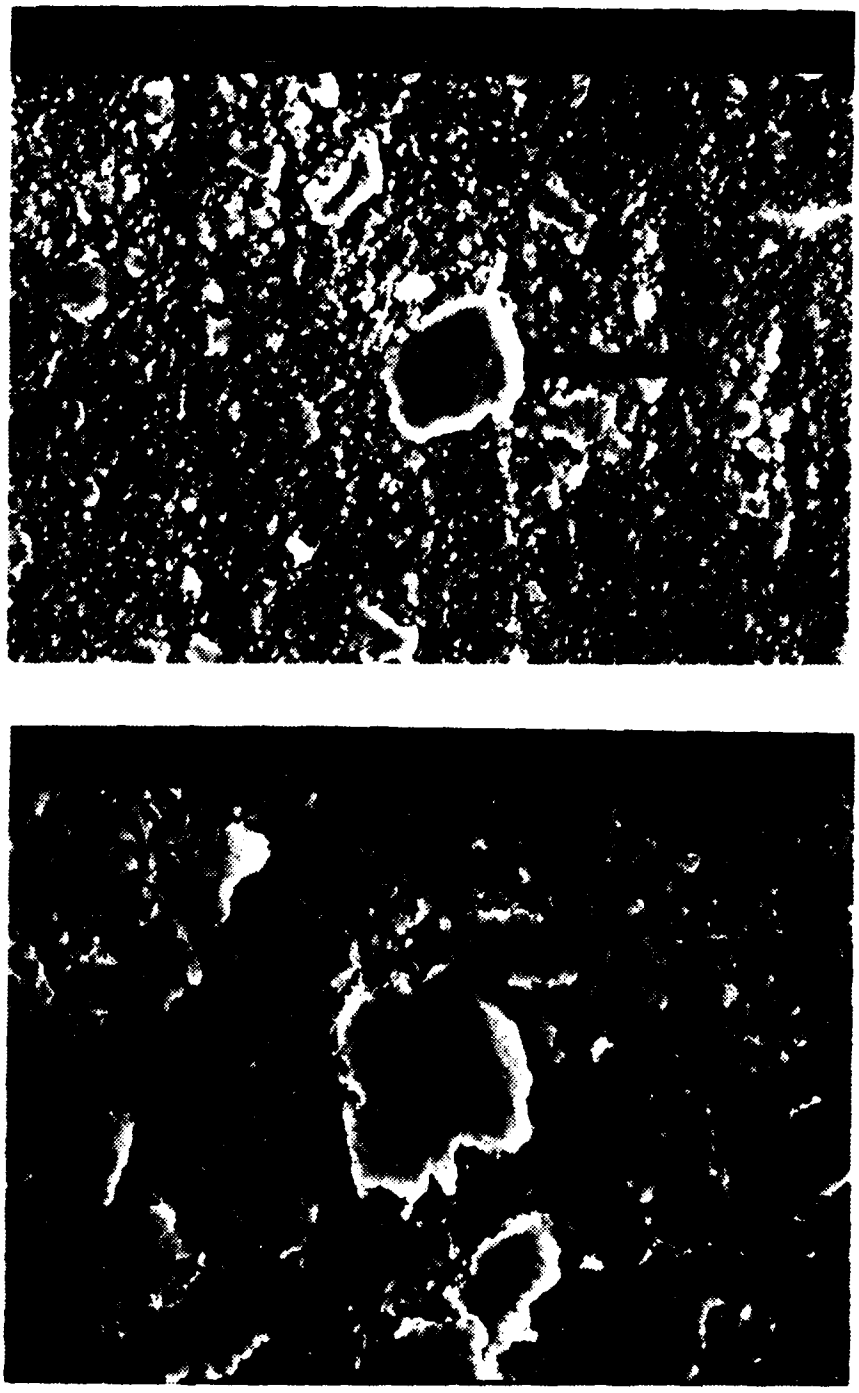

Figure 4.12. SEM micrographs showing the particles (denoted by arrows) for which spectra analysis was done.

TABLE VI

DATA FROM THE ANALYSIS OF PARTICLE 2-3-87-5
SHOWN IN FIGURE 4.13.

Quantification by chi-squared matching against standards

Standard	Chi-squared
trmc572826	11.72

ELEMENT	LINE	CONCENTRATION	ERROR	WINDOW (kev)
Be(Z= 4)	Kal	0.00	0.00	-0.01 - 0.19
Mg(Z=12)	Kal	15.41	0.60	1.14 - 1.34
Al(Z=13)	Kal	84.22	1.42	1.37 - 1.57
Si(Z=14)	Kal	0.04	0.00	1.63 - 1.83
Ti(Z=22)	Kal	0.01	0.00	4.40 - 4.60
Fe(Z=26)	Kal	0.12	0.00	6.29 - 6.49
Zr(Z=40)	Lal	0.20	0.06	1.93 - 2.13

TOTAL 100.00

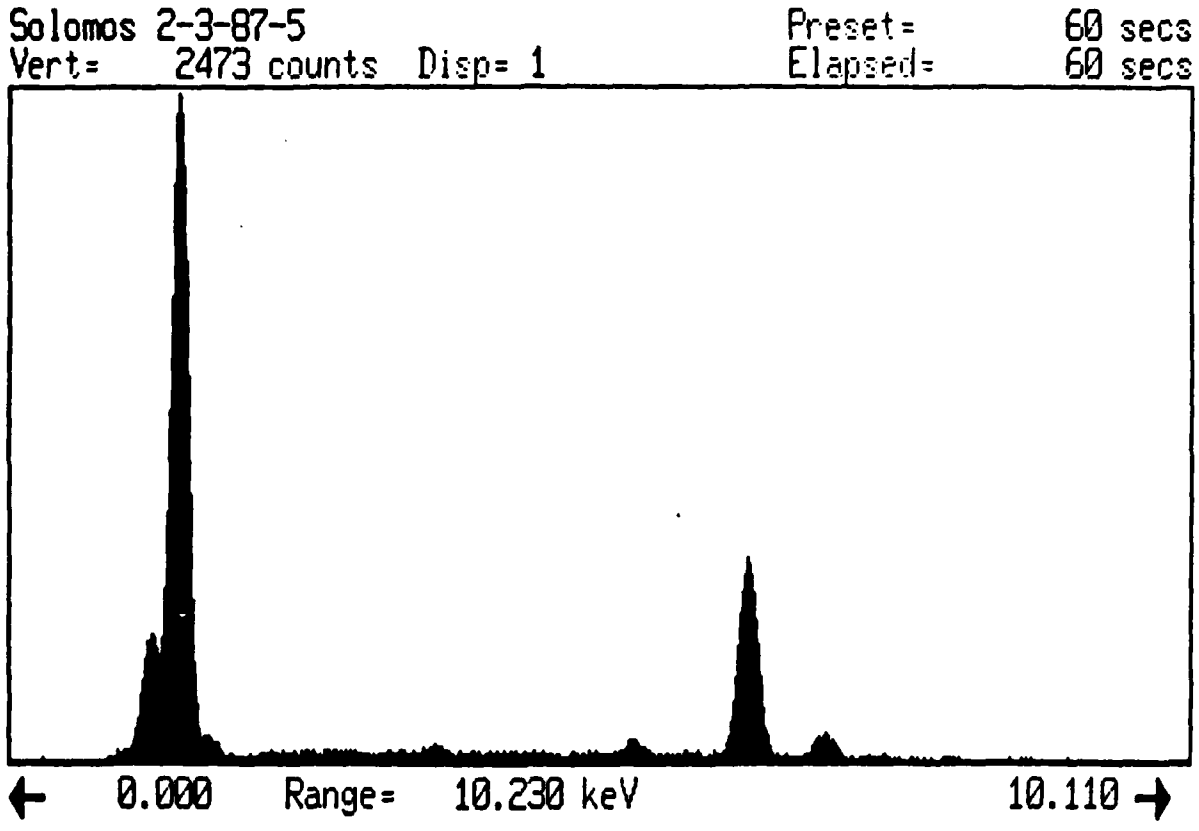

Figure 4.13. Graphical Analysis of Particle 2-3-87-5 Shown in Table VI.

TABLE VII

DATA FROM THE ANALYSIS OF PARTICLE 2-3-87-6
SHOWN IN FIGURE 4.14.

Quantification by chi-squared matching against standards

Standard	Chi-squared
S572826	1.99

ELEMENT	LINE	CONCENTRATION	ERROR	WINDOW (kev)
Be(Z= 4)	Kal	0.00	0.00	-0.01 - 0.19
Mg(Z=12)	Kal	16.94	0.40	1.14 - 1.34
Al(Z=13)	Kal	82.68	0.94	1.37 - 1.57
Si(Z=14)	Kal	0.01	0.01	1.63 - 1.83
Ti(Z=22)	Kal	0.01	0.00	4.40 - 4.60
Fe(Z=26)	Kal	0.02	0.00	6.29 - 6.49
Zr(Z=40)	Lal	0.34	0.06	1.93 - 2.13

TOTAL 100.004

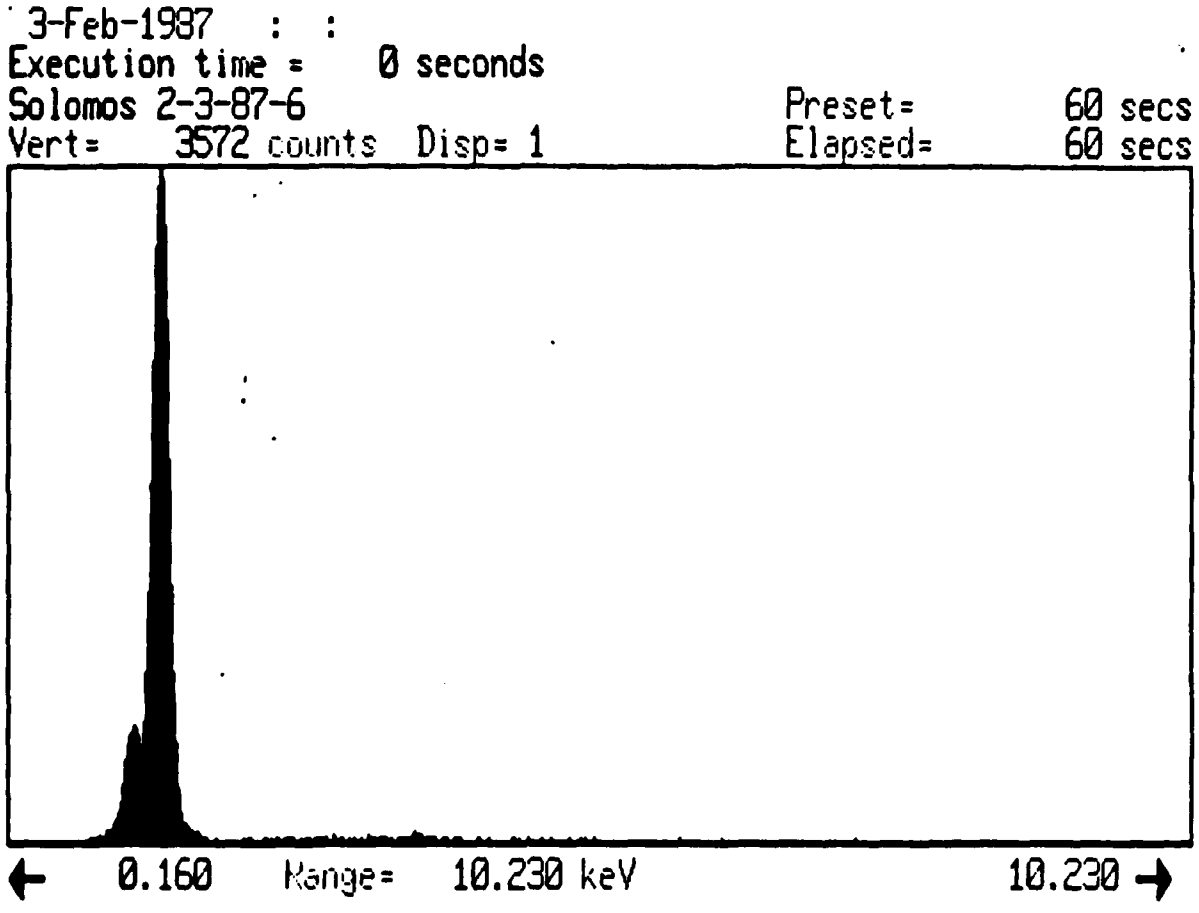

Figure 4.14. Graphical Analysis of Particle 2-3-87-6 Shown in Table VII.

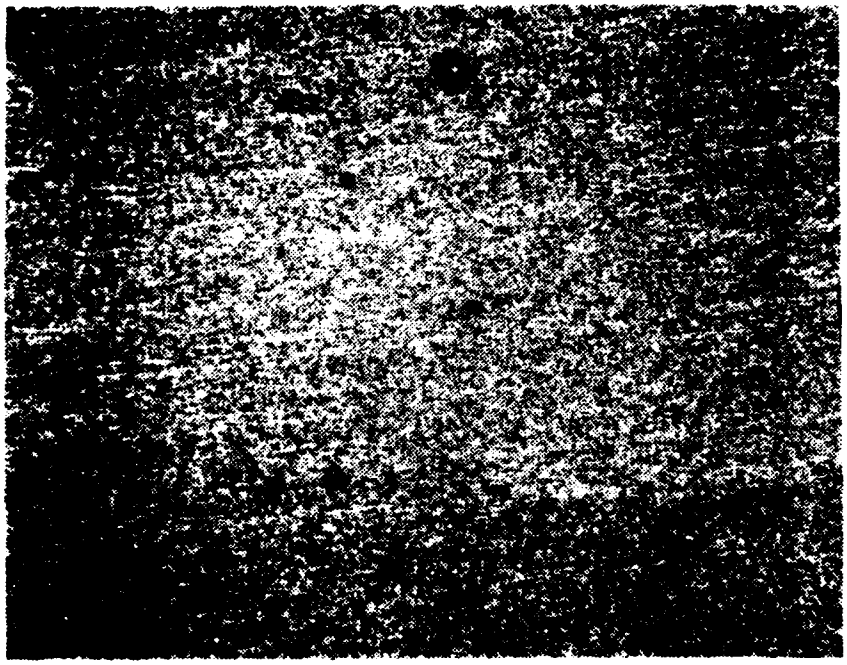

Figure 4.15. Optical micrograph taken from the simulated warm temperature deformed section, after electropolishing. 200X.

the structure is too confused and complicated by the β precipitate (Figure 4.16). For this reason and for a final experiment, the material was recrystallized by reheating the samples in a salt bath to 440°C for 2 minutes to be able to better see the distribution of the insoluble $ZrAl_3$ in the structure. Figures 4.17-4.20, which are SEM and corresponding optical micrographs taken near the fracture point, and 3 mm, 6 mm, and 10 mm from the point of the recrystallized sample, it is clear that the material is cavitated and void formation has taken place. However, there is no clear evidence for direct association of these voids with $ZrAl_3$ particles in them. In general we can say here that the material is showing a tendency toward void formation. Similar tendency was observed in Wise's material as shown in Figure 4.21. There was insufficient time to study in comparative sense the failure modes of Wise's work and these samples, to determine what is causing the void formation. A possibility here is that the grain structure is not fine enough, and so there is early onset necking because of the void formation on the sample and therefore lesser ductility. On the other hand, if the structure is really a fine one, then there should be the grain boundary sliding and the higher ductility, and this is evidence that in fact there is damage of the $ZrAl_3$ particles that will initiate void formation. At this point a more detailed

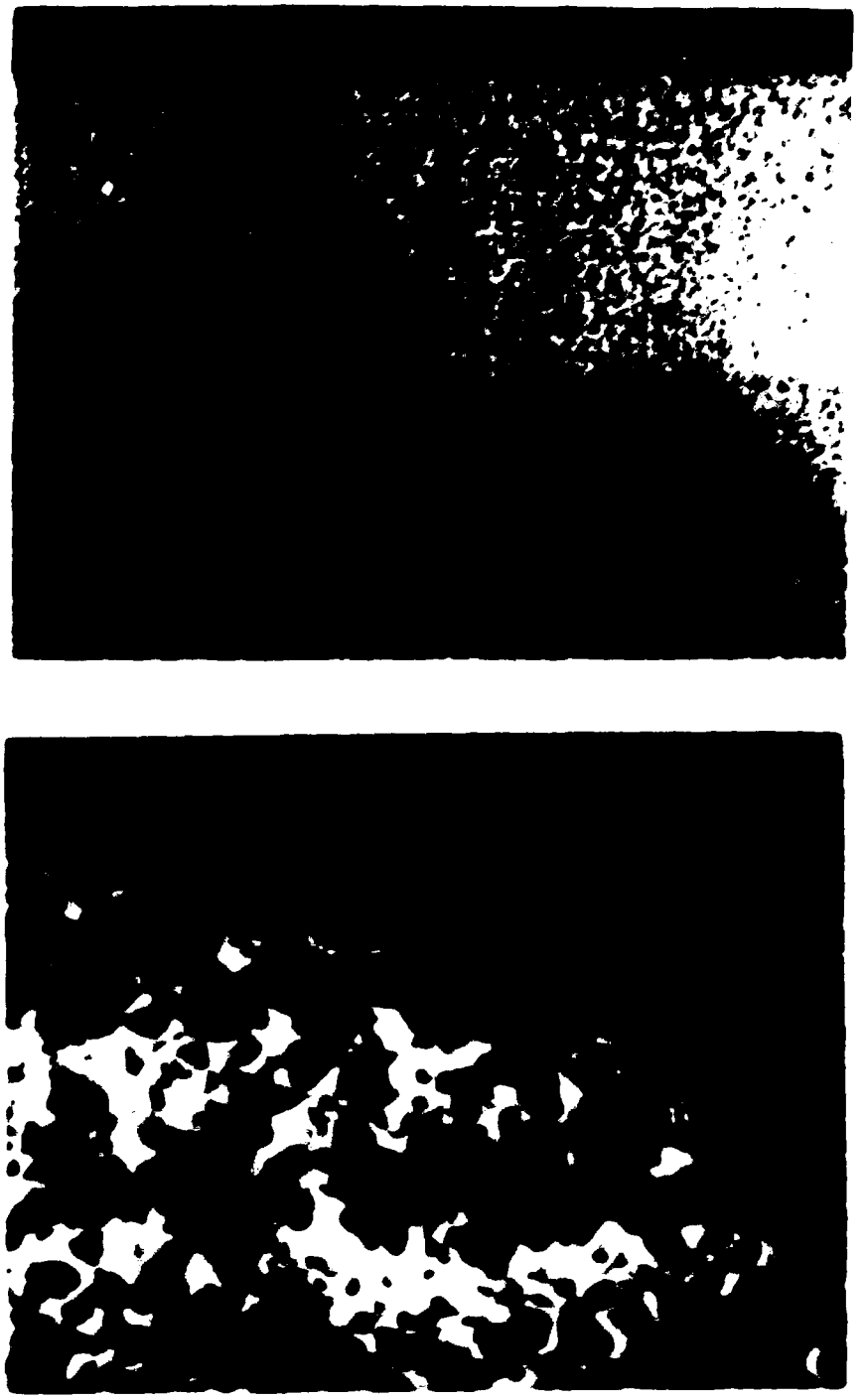

Figure 4.16. SEM micrographs of a simulated warm temperature deformed sample section after electropolishing and electroetching.

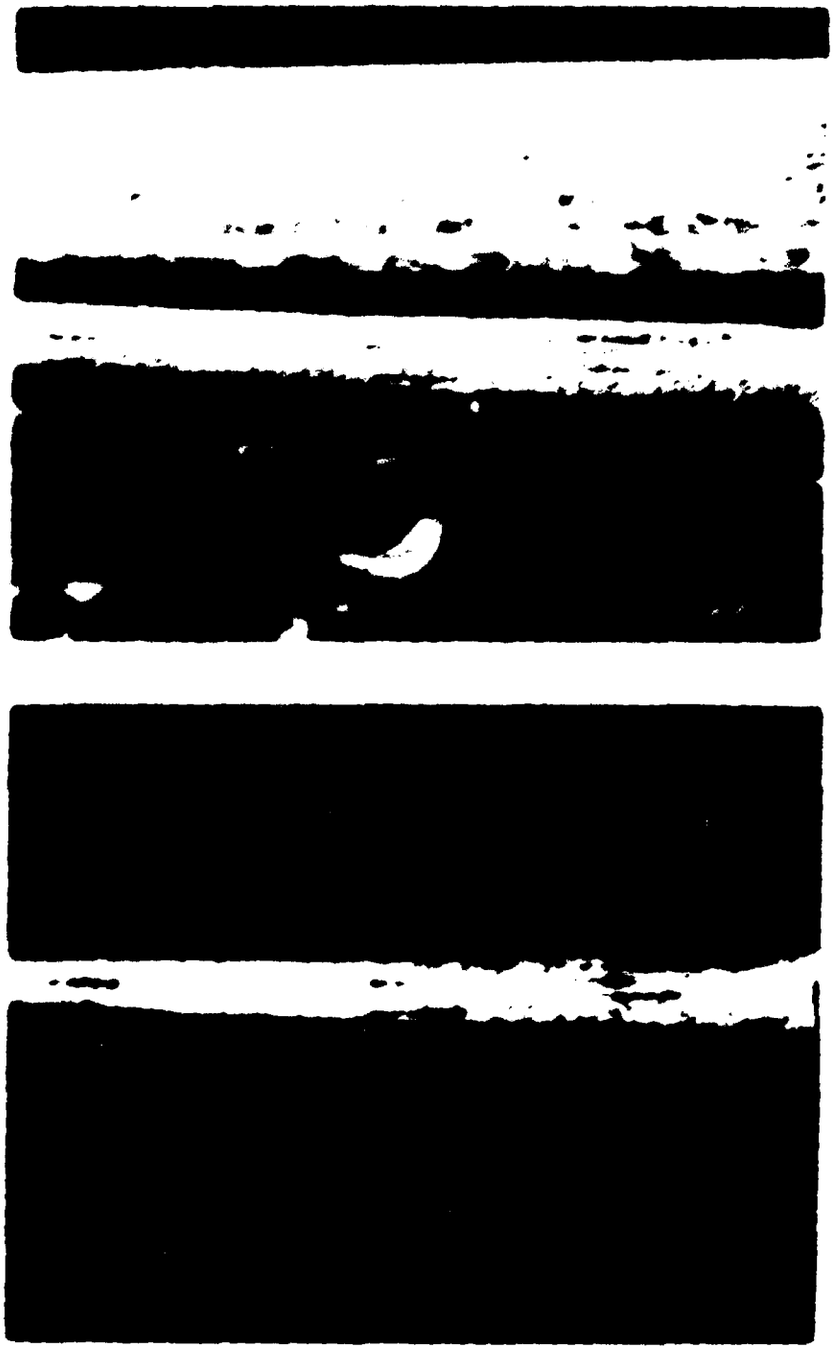

Figure 4.17. SEM micrograph (a) and optical micrograph b of the recrystalized simulated warm temperature deformed sample, near the tip. 200X.

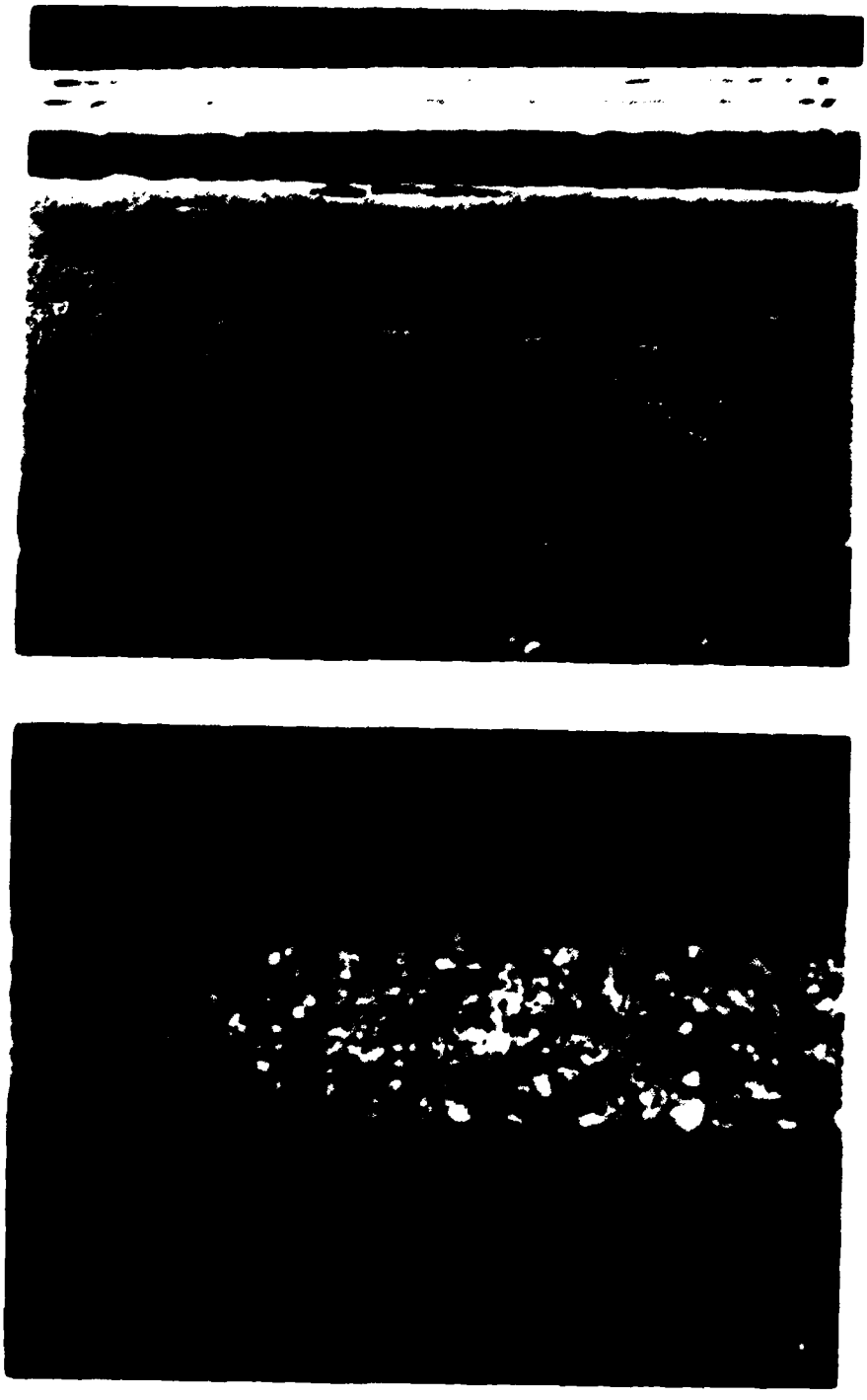

Figure 4.18. SEM micrograph (a) and optical micrograph (b) of the recrystallized simulated warm temperature deformed sample, 3 mm from the tip. 200X.

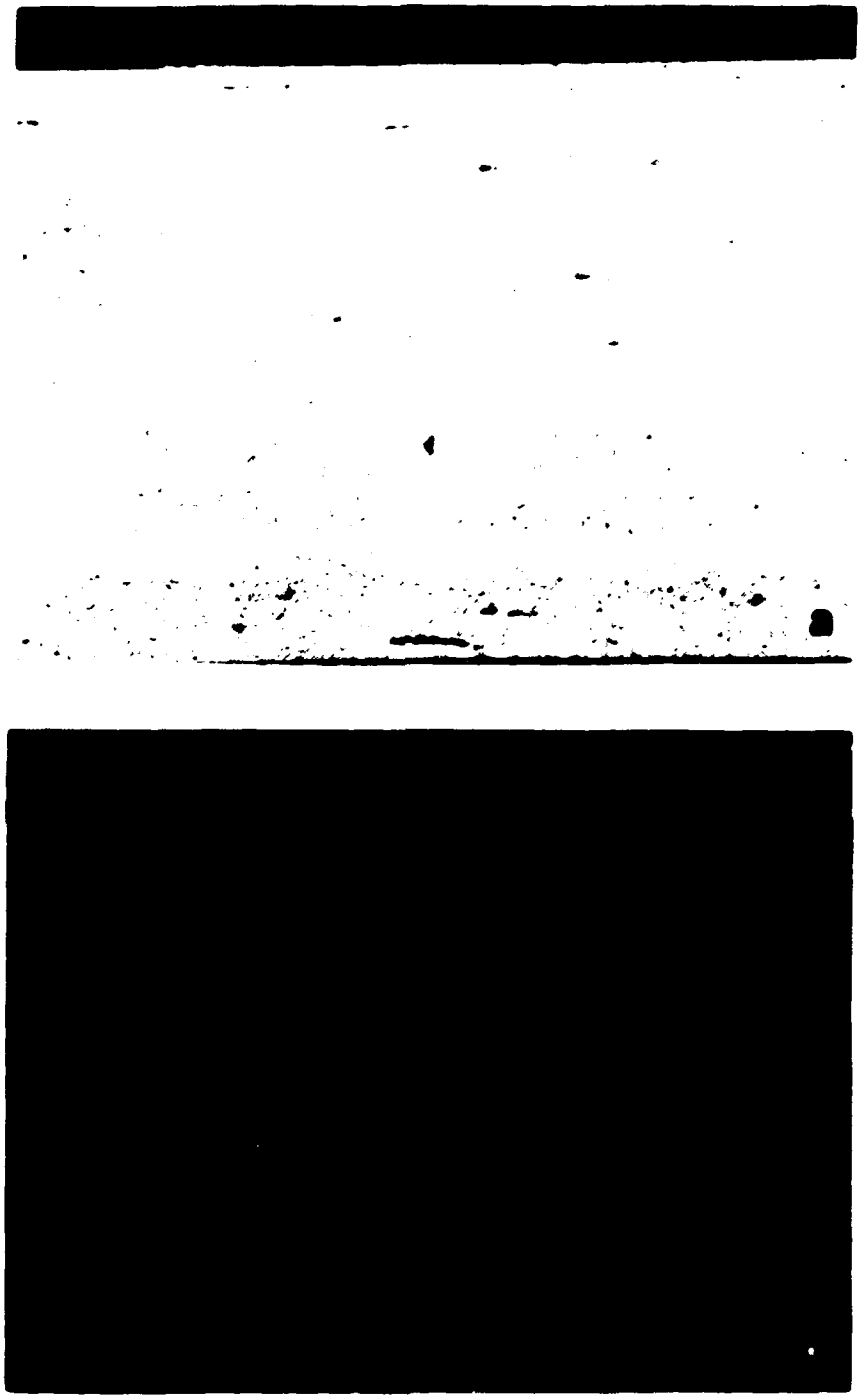

Figure 4.19. SEM micrograph (a) and optical micrograph (b) of the recrystallized simulated warm temperature deformed sample, 6 mm from the tip. 200X.

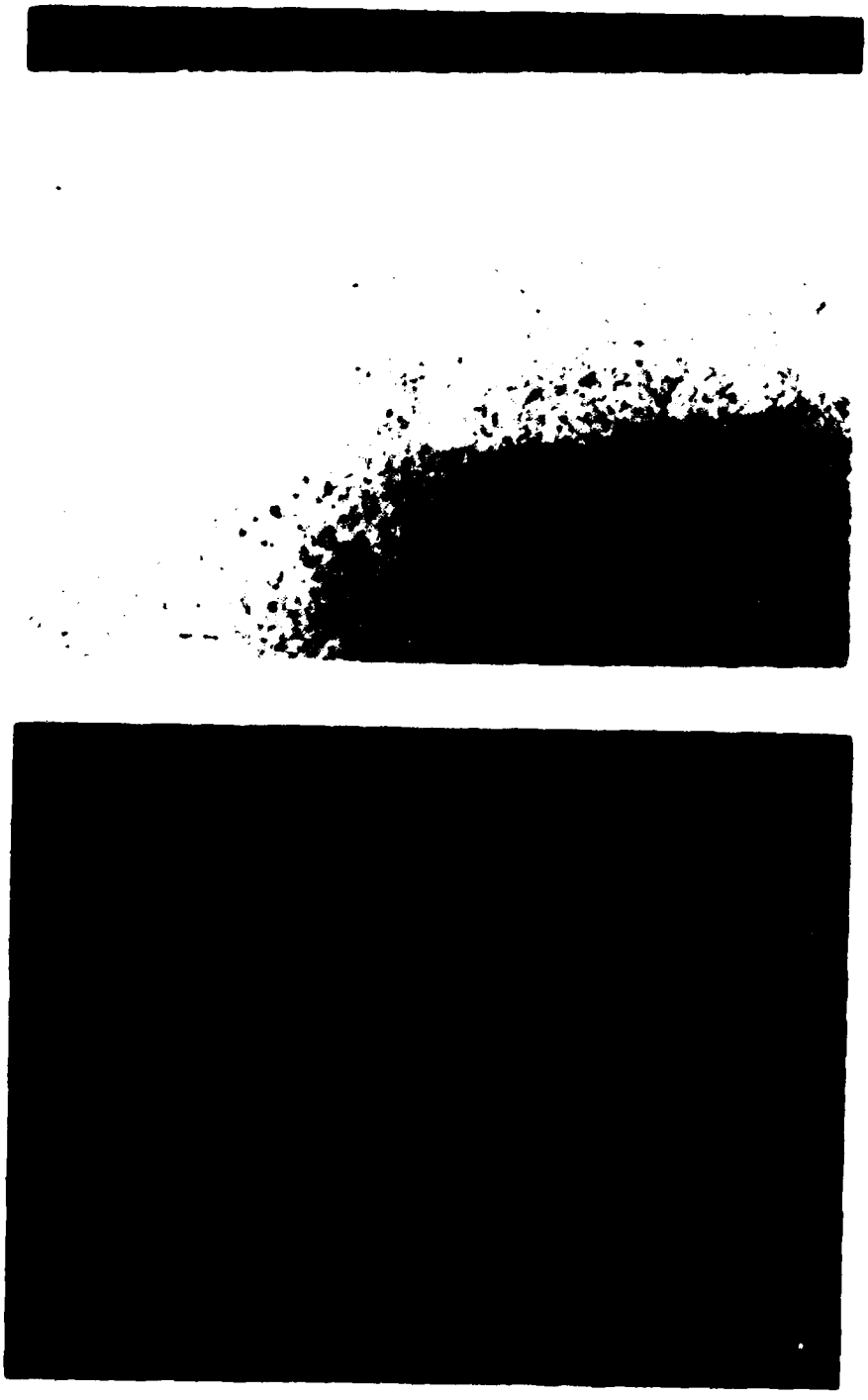

Figure 4.20. SEM micrograph (a) and optical micrograph (b) of the recrystallized simulated warm temperature deformed sample, 10 mm from the tip. 200X

Figure 4.21. SEM micrograph of Wise's [Ref. 35] sample, near the tip, after deformation to fracture at 300°C.

study by TEM of the nature of the grain boundaries is strongly recommended.

3. Ambient Temperature Mechanical Properties

For the ambient temperature tensile testing, specimens were cut from the gage portion of the simulated warm-deformed material. Specimen geometry was that of Figure 3.4. Due to the non-uniform thickness of the gage section, a portion of those specimens were milled to uniform thickness. The results of this testing are presented in Table VIII. In previous work done by Klankowski [Ref. 21] a wide variability in the ductilities was of serious concern, however, there was no discernible pattern to the scatter in the values obtained. Optical microscopy up to 800X did not provide any clues to the cause of the variability. In this work, since the samples had less superplastic ductility, they showed variation in thickness and therefore it was decided to remachine the samples to obtain a uniform thickness. It was seen that ductilities now became better and consistent with Klankowski's. Averaged data of previous and present work are presented in Table IX. The consistency is obvious, although the maximum ductility here was less than Klankowski's maximum. The main observation from those results in the lesser variability in the ductilities and the cause of the previous wide variability determined by Klankowski [Ref. 21] may be attributed to the omission of this aspect of specimen geometry. Therefore, the thickness

TABLE VIII

AMBIENT TEMPERATURE PROPERTIES OF Al-10%Mg-0.1%Zr SOLUTION TREATED AT 440°C AFTER SIMULATED SUPERPLASTIC FORMING.

SPECIMEN I.D.	σ_y (KPSI)	σ_y (MPA)	σ_u (KSPI)	σ_u (MPS)	% STRAIN MEASURED
S1a	37.7	260.0	50.6	348.9	2.5
S1b	38.2	263.4	53.4	368.2	2.8
S1c	36.3	250.3	58.0	399.9	5.3
S1d	37.9	261.3	56.9	392.3	5.0
S2a	41.3	284.8	57.2	394.4	5.0
S2b	36.1	248.9	52.5	362.0	3.8
S2c	37.3	257.2	58.4	402.7	5.1
After milled to uniform thickness					
S2d	36.5	251.7	60.5	417.1	5.3
S3a	36.4	251.0	65.6	452.3	7.1
S3b	37.1	255.8	65.2	449.5	6.9
S3c	37.1	255.8	68.2	471.6	8.5

TABLE IX

AMBIENT TEMPERATURE AVERAGED DATA OF Al-10%Mg-0.1%Zr AFTER SIMULATED SUPERPLASTIC FORMING.

	σ_y (KSPI)	σ_y (MPA)	σ_u (KSPI)	σ_u (MPA)	% STRAIN MEASURED AVERAGE	% STRAIN MEASURED VARIATION
(1)	38.5	265	55.2	380	4.2	2.5 TO 5.3
(2)	37.0	255	65.0	448	7.0	5.3 TO 8.5
(3)	38.6	266	64.6	445	6.8	2.0 TO 12.0

(1) present data, heavy reduction
(2) present data, heavy reduction, uniform thickness
(3) previous data, light reduction, Klankowski [Ref. 21]

as well as the lateral dimensions must be controlled to obtain consistent results.

V. CONCLUSIONS AND RECOMMENDATIONS

A. CONCLUSIONS

The following conclusions are drawn from this research.

1. The simulated superplastic forming was not successful in that less strain was attainable than anticipated from previous data, i.e., the idea that the heavier working scheme will enhance the ductility was not correct.
2. The ductility achieved is consistent with that reported by Wise and Salama and not, therefore, this research alone.
3. Transmission electron microscopy showed that the material possesses a very fine structure.
4. The simulated superplastic forming results in a material less ductile than one simply rolled and statically annealed.
5. It is necessary to give attention to the specimen thickness as well as the lateral dimensions for lesser ductility scatter.
6. The material is showing a tendency towards void formation.
7. Going to a little greater total strain, from ≈2 in Grider's work [Ref. 22] to 2.5 in present work

accounts for lesser ductility and higher ultimate strength at ambient temperature.

B. RECOMMENDATIONS

The following are recommendations for further study of the Al-10%Mg-0.1%Zr alloy.

1. Study in a comparative sense the failure modes of Wise [Ref. 35] and these samples to determine what is causing the void formation.
2. Further study by transmission electron microscopy, of the nature of the grain boundaries to assess if the lesser ductility is either because of void formation caused by the $ZrAl_3$, particles that they can be damaged by the heavy rolling or that the lesser ductility is in fact because of failure to achieve the fully recrystallized fine structure.

APPENDIX: COMPUTER PROGRAM

```
 10     INPUT "WHAT FILENAME.<FT> DO YOU WISH TO USE "; D$
 20     INPUT "SAMPLE ID..". ID$
 30     INPUT "SCALE FACTOR..", SCALE
 40     INPUT "CROSSECTIONAL AREA CU. IN..",AO
 50     INPUT "MAGNIFICATION RATION..",MAG
 60     OPEN "O", #1, DD$
 70     INPUT "ENTER THE LOAD,LBF..", F
 80     INPUT "ENTER X MEASURE FROM CHART, IN..", DELX
 90     S=F/AO
100     DELL=<DELX*SCALE)/MAG
110     E=DELL/1
120     SIGMA=S*(1+E)
130     EPSILON=LOG(1+E)
140     WRITE #1,F,DELX,S,E,SIGMA,EPSILON
150     INPUT "HIT RETURN TO CONT.,N NEW SPECIMEN,OR
        Q..",ANS$
160     IF ANS$="" GOTO 70
170     IF ANS$="N" THEN CLOSE #1:CLS:GOTO 10
180     IF ANS$="Q" THEN CLOSE #1:GOTO 190
190     END
```

LIST OF REFERENCES

1. Sherby, O.D. and Wadsworth, J., "Development and Characterization of Fine-Grained Superplastic Materials," Deformation Processing and Structure, G. Krauss, ed., American Society for Metals, Metals Park, Ohio (1984), pp. 355-390.

2. Bengough, G.D., Journal of the Institute of Metals, Vol. 7 (1912), pp. 123-146.

3. Rosenhain, W. Haughton, J.L. Bingham, K.E., Journal of the Institute of Metals, Vol. 23 (1920), p.261.

4. Pearson, C.E., "The Viscous Properties of Extruded Eutectic Alloys of Lead-Tin and Bismuth-Tin," Journal of the Institute of Metals, Vol. 54 (1934), pp. 111-134.

5. Higashi, K., Oknishi, T. and Nakatani, Y., "Superplastic Behavior of Commercial Aluminum Bronze," Scripta Metallurgica, Vol.19 (1985), pp. 821-823.

6. Hess, F.G., Jr., High Strength to Weight Aluminum-18 Weight Percent Magnesium Alloy Through Thermomechanical Processing, M.S. Thesis, Naval Postgraduate School, Monterey, California, December 1976.

7. Bingay, C.P., Microstructural Response of Aluminum-Magnesium Alloys to Thermomechanical Processing, M.S. Thesis, Naval Postgraduate School, Monterey, California, December 1977.

8. [illegible] T.L., Effects of Thermomechanical Processing of Aluminum-Magnesium Alloys Containing High Weight Percent Magnesium, M.S. Thesis, Naval Postgraduate School, Monterey, California, December 1977.

9. [illegible] A., High Strength Aluminum-Magnesium Alloys: Thermomechanical Processing, Microstructure and Tensile Mechanical Properties of High Strength Aluminum-Magnesium Alloys, M.S. Thesis, Naval Postgraduate [illegible] Monterey, California, March 1980.

10. [illegible] An Investigation into the Influence of Thermomechanical Processing on Microstructure and Mechanical Properties of High Strength Aluminum-Magnesium Alloys, M.S. Thesis, Naval Postgraduate [illegible] California, December 1977.

11. Chesterman, C.W., Jr., Precipitation, Recovery and Recrystallization Under Static and Dynamic Conditions for High Magnesium Aluminum-Magnesium Alloys, M.S. Thesis, Naval Postgraduate School, Monterey, California, March 1980.

12. Johnson, R.B., The Influence of Alloy Composition and Thermomechanical processing Procedure on Microstructural and Mechanical Properties of High-Magnesium Aluminum Alloys, M.S. Thesis, Naval Postgraduate School, Monterey, California, June 1980.

13. Shirah, R.H., The Influence of Solution Time and Quench Rate on the Microstructure and Mechanical Properties of High Magnesium Aluminum-Magnesium Alloys, M.S. Thesis, Naval Postgraduate School, Monterey, California, March 1980.

14. Becker, J.J., Superplasticity in Thermomechanically Processed High-Magnesium Aluminum Magnesium Alloys, M.S. Thesis, Naval Postgraduate School, Monterey, California, March 1984.

15. Mills, M.E., Superplasticity in Thermomechanically Processed Aluminum-10.2%Mg-0.52%Mn Alloy, M.S. Thesis, Naval Postgraduate School, Monterey, California, September 1984.

16. Stengel, A.R., Effects of Annealing Treatments on Superplasticity in a Thermomechanically Processed Aluminum-10.2%Mg-0.52%Mn Alloy, M.S. Thesis, Naval Postgraduate School, Monterey, California, December 1984.

17. Self. R.J., The Effect of Alloy Additions on Superplasticity in Thermomechancially Processed High Magnesium Aluminum Magnesium Alloys, M.S. Thesis, Naval Postgraduate School, Monterey, California, December 1984.

18. Alcamo, M.E., Effect of Strain and Strain Rate of Microstructure of a Superplastically Deformed Al-10%Mg-0.1%Zr Alloy, Mechanical Engineer Thesis, Naval Postgraduate School, Monterey, California, June 1985.

19. Berthold, D.B., Effect of Temperature and Strain Rate on the Microstructure of a Deformed, Superplastic Al-10%Mg-0.1Zr Alloy, M.S. Thesis, Naval Postgraduate School, Monterey, California, June 1985.

20. Hartman, T.S., Mechanical Characteristics of a Superplastic Aluminum 10%Mg-0.1Zr Alloy, M.S. Thesis, Naval Postgraduate School, Monterey, California, June 1985.

21. Klankowski, K.A., Retained Ambient Temperature Properties of Superplastically Deformed Al-10%Mg-0.1Zr, Al-10%Mg-0.5%Mn and Al-10%Mg-0.4%Cu Alloys, M.S. Thesis, Naval Postgraduate School, Monterey, California, December 1985.

22. Grider, W.H., The Effect of Thermomechanical Processing Variables on Ductility of a High-Mg, Al-Mg-Zr Alloy, M.S. Thesis, Naval Postgraduate School, Monterey, California, June 1986.

23. Wert, J.A., "Thermomechanical Processing of Heat-Treatable Aluminum Alloys for Grain Size Control," Conference Proceedings of TMS-AIME, pp. 67-94, February 1985.

24. McNelley,T.R., Lee, E.-W. and Mills, M.E., "Superplasticity in a Thermomechanically Processed High-Mg, Al-Mg Alloy," Metallurgical Transactions A, Vol. 17A (1986), pp. 1035-1041.

25. Lee, E.-W., McNelley, T.R. and Stengle, A.F., "The Influence of Thermomechanical Processing Variables on Superplasticity in a High-Mg, AlMg Alloy," Metallurgical Transactions A, Vol. 17A (1986), pp. 1043-1050.

26. McNelley, T.R. and Garg, A., "Development of Structure and Mechanical Properties in Al-10.2 Wt. Pct. Mg by Thermomechanical Processing," Scripta Metallurgica, Vol. 18 (1984), pp. 917-920.

27. Wadsworth, J., Petoy, A.R., Lewis, R.E., "Superplastic Al-Cg-Li-Mg-Zr Alloys," Metallurgical Transactions A., Vol 16A, pp 2319-2332, December 1985.

28. Asby, M.F. and Verrall, R. A., "Diffusion-Accommodated Flow and Superplasticity," Acta Metallurgica, Vol. 21 (1973), pp. 149-163.

29. Ruano, O.A., and Sherby, O.D., "Low Stress Creep of Fine-Grain Boundary Sliding?," Material Science and Engineering, Vol. 56 (1982), pp. 167-175.

30. Weertman, J., J. Appl. Physics, Vol. 26 (1955), p. 1213.

31. Weertman, J., J. Appl. Physics, Vol. 28 (1957), pp. 1185-1189.

32. Smallman, R.E., Modern Physical Metallurgy, 4th Ed. (1985) pp. 363-366, Butterworths.

33. Alcoa Technical Center, Ltr., August 1984.

34. Dieter, G.E., Materials Science and Engineering Series, McGraw-Hill (1976).

35. Wise, J., The Influence of Total Strain, Rate of Straining and Reheating Time During Warm Rolling on the Superplastic Ductility of an Al-Mg-Zr Alloy. M.S. Thesis, Naval Postgraduate School, Monterey, California, March 1987.

36. Gifkins, R.C., "Mechanisms for Superplasticity," Superplastic Forming of Structural Alloys, N.E. Paton and C.H. Hamilton, eds., The Metallurgical Society of AIME, Warrendale, Pennsylvania (1982), pp. 3-26.

37. Metals Handbook, 9th ed., Vol. 9 (1985), pp. 351-360, American Society for Metals.

INITIAL DISTRIBUTION LIST

	No. Copies
1. Defense Technical Information Center Cameron Station Alexandria, Virginia 22304-6145	2
2. Library, Code 0142 Naval Postgraduate School Monterey, California 93943-5002	2
3. Department Chairman, Code 69Mx Department of Mechanical Engineering Naval Postgraduate School Monterey, California 93943-5000	1
4. Professor T.R. McNelley, Code 69Mc Department of Mechanical Engineering Naval Postgraduate School Monterey, California 93943-5000	5
5. Dr. Steve J. Hales, Code 69He Department of Mechanical Engineering Naval Postgraduate School Monterey, California 93943-5000	1
6. Dr. Lewis Sloter, Code AIR 931A Headquarters, Naval Air Systems Command Washington, D.C. 20361	1
7. Jeff Waldman Naval Air Development Center Materials Science Department Warminster, Pennsylvania 18974	1
8. Dr. Eu Whee Lee Naval Air Development Center Materials Science Department Warminster, Pennsylvania 18974	1
9. Hellenic Navy General Staff 2nd Branch, Education Department Stratopedan Papagou GR 155.61 - Holargos, GREECE	4
10. CDR. Dimosthenis K. Solomos Themistokleous 36-38 Ag. Paraskevi 153.42 ATHENS - GREECE	5

END

8-87

DTIC